



HAL
open science

A genetic algorithm-based topology optimization (GATO) method for convective cooling of a heating surface with multiple heat sources

Yijun Li, Stéphane Roux, Cathy Castelain, Yilin Fan, Lingai Luo

► To cite this version:

Yijun Li, Stéphane Roux, Cathy Castelain, Yilin Fan, Lingai Luo. A genetic algorithm-based topology optimization (GATO) method for convective cooling of a heating surface with multiple heat sources. *International Journal of Heat and Mass Transfer*, 2024, 224, pp.125349. 10.1016/j.ijheatmasstransfer.2024.125349 . hal-04487946

HAL Id: hal-04487946

<https://hal.science/hal-04487946>

Submitted on 27 Mar 2024

HAL is a multi-disciplinary open access archive for the deposit and dissemination of scientific research documents, whether they are published or not. The documents may come from teaching and research institutions in France or abroad, or from public or private research centers.

L'archive ouverte pluridisciplinaire **HAL**, est destinée au dépôt et à la diffusion de documents scientifiques de niveau recherche, publiés ou non, émanant des établissements d'enseignement et de recherche français ou étrangers, des laboratoires publics ou privés.

A genetic algorithm-based topology optimization (GATO) method for convective cooling of a heating surface with multiple heat sources

Yijun LI, Stéphane ROUX, Cathy CASTELAIN, Yilin FAN^{*}, Lingai LUO[†]

*Nantes Université, CNRS, Laboratoire de thermique et énergie de Nantes, LTeN, UMR6607, F-44000
Nantes, France*

Abstract

The heat-generating surface with multiple heat sources is frequently encountered in modern power electronic devices. Efficient cooling techniques are especially needed to prevent the overheating of these devices, so as to avoid consequences like performance deterioration, failure rate increase, reduced lifetime and safety threats. The main objective of this study is to design and optimize the structure of heat sinks for single-phase convective cooling of a heat-generating surface under multiple-peak heat flux. In particular, a genetic algorithm-based topology optimization (GATO) method has been developed and tested for this purpose. The middle area of the heat sink receiving heat flux is treated as the design domain and represented as a binary matrix ($M_{row \times column}$). Each element in the matrix is considered either as fluid or as solid, and their allocation is optimized to minimize the peak temperature (T_{peak}) at the heating surface of the heat sink under the constraint of constant void volume for the fully-connected fluid domain. For each optimization step, the fluid flow and temperature characteristics are obtained by CFD simulation using OpenFoam and the GA operations (selection, crossover, mutation, etc.) are applied. The impacts of design and operation parameters on the optimized global flow channel configuration are evaluated, including the heat flux shape, the fluid void fraction, the inlet velocity, and the resolution of the design domain.

The results obtained show that: (1) the proposed GATO method could successfully determine the optimal flow channel configuration of the heat sink, minimizing the T_{peak} at the heating surface; (2) The optimized flow channel configuration depends on the design and operating parameters while the effectiveness and robustness of the GATO method are verified; (3) Compared to conventional straight channel heat sink, the GATO heat sink could always provide a better cooling performance under the same working condition, with a reasonable and acceptable increase of the pressure drop. The method developed in study could be a useful contribution to the TO of heat sinks/exchangers with demonstrated potential in engineering thermal design and optimization.

Keywords: Heat sink, Topology optimization (TO), Genetic algorithm (GA), Multiple-peak heat flux, Flow channel configuration, Convective cooling

^{*} Corresponding author. E-mail address: yilin.fan@univ-nantes.fr (Y. Fan)

[†] Corresponding author. E-mail address: lingai.luo@univ-nantes.fr (L. Luo)

1 Nomenclature

Latin letters

| | |
|-----------|--|
| A | Surface area [m^2] |
| B | Constant of heat flux formula [$\text{W}\cdot\text{m}^{-2}$] |
| C_p | Specific heat [$\text{J}\cdot\text{kg}^{-1}\cdot\text{K}^{-1}$] |
| D_h | Hydraulic diameter [m] |
| E | Energy [J] |
| e | Channel thickness [m] |
| F | External force [N] |
| g | Gravitational acceleration [$\text{m}\cdot\text{s}^{-2}$] |
| H | Specific enthalpy [$\text{J}\cdot\text{kg}^{-1}$] |
| h_{avg} | Average heat transfer coefficient [$\text{W}\cdot\text{m}^{-2}\cdot\text{K}^{-1}$] |
| k | Generation number |
| L | Length [m] |
| M | Matrix [-] |
| \dot{m} | Mass flow rate [$\text{kg}\cdot\text{s}^{-1}$] |
| Nu | Nusselt number [-] |
| p | Pressure [Pa] |
| P^* | Normalized pressure drop [-] |
| Q | Heating power [W] |
| q | Heat flux [$\text{W}\cdot\text{m}^{-2}$] |
| Re | Reynolds number [-] |
| R_{th} | Thermal resistance [$\text{K}\cdot\text{W}^{-1}$] |
| S_w | Wetted surface area of the flow channels in the design domain [m^2] |
| T | Temperature [K] |
| T^* | Normalized temperature [-] |
| v | Velocity [$\text{m}\cdot\text{s}^{-1}$] |
| v^* | Normalized velocity [-] |
| V_{ch} | Wetted volume of flow channels in the design domain [m^3] |
| w | Width [m] |
| x, y, z | Axis |

Greek symbols

| | |
|------------|---|
| ρ | Density [$\text{kg}\cdot\text{m}^{-3}$] |
| Φ | Void fraction [-] |
| τ | Shear stress [$\text{N}\cdot\text{m}^{-1}$] |
| σ | Spatial spread of the heat peak [mm] |
| ΔP | Pressure drop [Pa] |
| λ | Thermal conductivity [$\text{W}\cdot\text{m}^{-1}\cdot\text{K}^{-1}$] |

Superscripts/subscripts

| | |
|-----------|----------------------------------|
| 0 | Reference value |
| avg | Average value |
| c | Column of matrix |
| ch | Channel |
| col | Collector |
| $design$ | Design domain |
| dis | Distributor |
| eff | Effective |
| $element$ | Elements in a binary matrix |
| f | Fluid |
| in | Inlet |
| k | Generation number |
| max | Maximum value |
| $median$ | Median value |
| $middle$ | Middle |
| min | Minimum value |
| out | Outlet |
| $peak$ | Peak value |
| r | Row of matrix |
| s | Solid part of heat sink material |
| sw | Separating wall between channels |
| T | Temperature |
| tot | Total |
| w | Wall |

Abbreviations

| | |
|-------|---|
| CCIPL | Centre de calcul intensif Pays de la Loire |
| CFD | Computational Fluid Dynamics |
| EA | Evolutionary Algorithm |
| FVM | Finite Volume Method |
| GATO | Genetic Algorithm-Based Topology Optimization |
| HF | Heat Flux |
| HPC | High performance computing |
| MCMs | Multi-chip modules |
| NSGA | Non-dominated Sorting Genetic Algorithm |
| RSC | Reference Straight Channel |
| STD | Standard Deviation |

2

3

1 **I. Introduction**

2 A heat generating surface with multiple heat sources can be commonly found in modern
3 electronic and power devices, including multi-chip modules (MCMs) [1,2], Lithium-ion battery
4 packs [3], multi-junction high concentrator photovoltaics [4] and many others. The array
5 architecture of unit functional components will increase the overall output, capacity or
6 performances of these devices on one hand, and cause the highly heterogeneous and
7 multiple-peak type generated heat flux on the other hand. If not properly cooled, the higher
8 junction temperature due to the overheating would deteriorate the performance/capacity and
9 reduce their lifetime [5,6], a problem frequently encountered due to ever-increasing integration
10 level (compactness) and power density. Still worse is the existence of local hotspots due to
11 this heterogeneous heat generation [7,8], more likely to appear than under uniform heating or
12 single heat source conditions, resulting in more serious consequences such as the device
13 failure or thermal runaway. As a result, the thermal management of these devices has become
14 an essential but challenging issue in order to maintain a suitable range of working temperature,
15 and above all, to guarantee the lower junction temperature below a threshold value.

16
17 Among various cooling techniques, the single-phase liquid cooling (usually water) by forced
18 convection using heat sinks has been broadly applied in the thermal management of small and
19 high-power devices owing to its high heat transfer capability and compact size [9]. A number
20 of factors may influence the cooling performance of heat sink, and among them, the internal
21 structure or the channel configuration determines the flow path patterns, therefore should be
22 carefully designed [10]. Many channel configurations have been proposed and used for heat
23 sinks, including parallel straight channel, wavy channel, pin-fin or oblique-fin structure, double-
24 layered structure, and others [11]. To further enhance the heat transfer, abundant studies have
25 been conducted on the structure optimization using computational fluid dynamics (CFD)
26 simulation and numerical algorithms. However, most of them are focused on the size or shape
27 optimization or investigation of certain geometrical elements (e.g., headers/manifolds [12],
28 fins/obstacles [13], inlets [14], etc.) based on a predefined geometry, insufficient to handle
29 more complex problems such as for the efficient cooling of a highly heterogeneous heating
30 surface. In contrast, the topology optimization (TO) treats this problem in a different way by
31 acting directly on the global spatial distribution of fluid and solid materials and their connectivity
32 in a certain design domain [15,16]. Theoretically, it can attain any possible flow configuration
33 corresponding to the defined optimization objective(s) and under some constraints. In this
34 sense, the TO has the highest degrees of freedom, capable of proposing complex but highly
35 efficient designs without being limited to the prescribed geometry [17]. Being considered as a
36 groundbreaking technique, it has attracted great attention in recent years [18,19].

1 The process of TO for heat sinks generally includes four basic stages [20]: (1) design
2 parametrization, (2) heat transfer modeling, (3) optimization process, and (4) final realization.
3 Currently, a combination of the density-based method, the finite element modeling, and the
4 gradient-based optimizer is the mainstream in the TO of heat sinks/heat exchangers [20]. It
5 has shown good efficiency in handling optimization problems with a high number of design
6 variables [19,21]. Nevertheless, the implementation of such TO strategy may encounter some
7 difficulties in handling numerical artifacts or descriptions of clear solid-fluid interfaces, and
8 more importantly, it may be easily trapped into a local optimum [22]. Hence, some novel,
9 gradient-free approaches, like genetic algorithm (GA) and Bayesian optimization become to
10 be considered, as an alternative way, to overcome these deficiencies and converges towards
11 a global optimum [23].

12
13 The GA is a stochastic evolutionary algorithm (EA) that mimics the biological evolution of
14 species based on chromosomes and genes [24]. Merited by its robustness to the global
15 optimum and good fitness to multi-objective optimization, it has been developed and used by
16 many researchers for the optimization of heat transfer, including both conduction and
17 convection problems [25,26]. As for heat sinks, GA has been mainly involved in the parameter
18 or shape optimization of some local enhancement element in the channel. But it has rarely
19 been implemented in TO mainly due to the high computational cost. A limited number of
20 attempts have been made in recent years. Among them, Yoshimura et al. [27] proposed a
21 Kriging surrogate model-assisted GA method on single-/multi-objective TO of cooling flow
22 channel configurations. Later, the NSGA-II method has been coupled with the Kriging
23 surrogate model to search for better designs of lattice-structured heat sinks regarding thermal
24 performance and material cost [28]. Mekki et al. [29,30] developed and tested a GA-based TO
25 method for thermo-fluid equipment in aerospace applications, but only the elementary fin
26 shapes have been focused on using voxel representation. Weber et al. [31] also used GA
27 method to optimize the shape/topology of a heat exchanger fin, and best designs could be
28 achieved when coupled with free form deformation. Yaji et al. [32] proposed a hybrid data-
29 driven multi-fidelity topology design combining both density-based methods for the low-fidelity
30 TO and NSGA-II to select the optimal Pareto front. Nevertheless, none of the GA studies
31 addresses the TO of global flow channel configuration in heat sinks. Moreover, the majority of
32 the above-mentioned TO studies deal with the simplified 2D or pseudo-3D design domain (e.g.,
33 [33]). For those studies with 3D parametrization (e.g., [34,35]), most of them are performed
34 under uniform heating , with only several exceptions addressing more complex (but more
35 realistic) heating boundaries with multiple heat sources [36] or shifted thermal loads [37].

1 Being motivated by the remaining research gaps to fill, we develop in this work a *GA-based*
2 *TO (GATO) method to optimize the global flow channel configuration of the heat sink for the*
3 *forced-convection cooling of a heating surface under multiple-peak heat flux*. Different from
4 other studies existing in the literature, the pseudo-3D design domain of the heat sink is
5 represented by a binary matrix in a direct explicit way, each element being either solid (0) or
6 fluid (1). Consequently, the TO problem of flow channel configuration in the design domain
7 becomes then the search for the best allocation of 0 and 1 elements in the matrix. A 3D finite
8 volume method (FVM) solver is used for the modeling of conjugate heat transfer and fluid flow
9 for each design. The GA method is used as the optimizer to renew the design variables
10 (matrices) to minimize the peak temperature of the heating surface (T_{peak}) under the specific
11 constraint of constant void fraction for the fully connected fluid domain. In more detail, the local
12 features (genes) that contribute to the lowered T_{peak} value would be maintained in successive
13 generations while those that bring about worse results would be discarded, a procedure
14 analogizing the mechanism of natural selection as the “*survival of the fittest*”. One generation
15 after another will converge to the optimized flow channel configuration that has the lowest T_{peak}
16 on the heating surface. This TO method combining direct explicit parametrization, FVM, and
17 GA, inspired and developed from the pioneering works of Boichot et al. [38,39] on the pure
18 conduction optimization problem, has never been used for the convection cooling of a heating
19 surface under multiple heat sources to the best of our knowledge.

20
21 The remaining parts of this paper are organized as follows. Section 2 introduces the
22 methodology with detailed description for each step of the GATO algorithm. In section 3, the
23 optimization results of a benchmark heat sink design are presented and discussed. A
24 comprehensive parametric study evaluating the influences of different design variables is
25 reported in section 4. Section 5 provides further discussions on some interesting issues and
26 comments on the advantages and limitations of this method. Finally, the main conclusions and
27 following work are summarized in section 6.

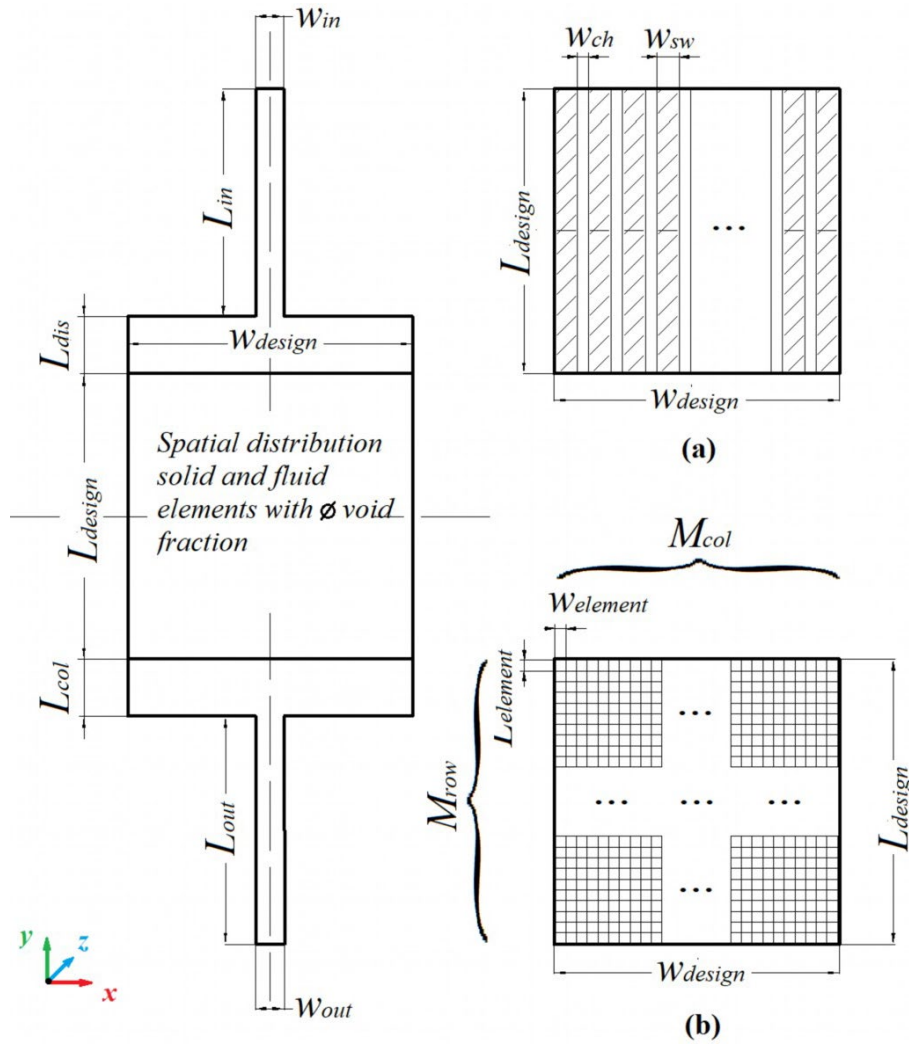
28 29 **2. Methodology**

30 **2.1 Heat sink model**

31 Figure 1 shows a representative schematic view of the heat sink geometry for this study. It has
32 a single inlet (and outlet) straight channel of w_{in} (w_{out}) in width and L_{in} (L_{out}) in length, both
33 aligned with the centerline of the heat sink. In between the inlet/outlet tubes is a rectangular
34 cuboid having overall dimensions of L_{middle} in length (y direction), w_{design} in width (x direction),
35 and e in depth (z -direction). This core part of the heat sink consists of 3 sections: the inlet
36 manifold ($w_{design} \times L_{dis}$), the middle flow channel domain ($w_{design} \times L_{design}$), and the outlet

1 manifold ($W_{design} \times L_{col}$). Note that all the flow channels are coplanar with the same channel
 2 depth of e , rendering it a pseudo-3D fluid domain adapted for design parametrization. Only the
 3 upper surface of the flow channel domain (heating surface with a surface area of A_{design})
 4 receives a non-uniform multiple-peak heat flux while all other surfaces enclosing the heat sink
 5 are considered as adiabatic walls. In that way, the total amount of heat generated will be
 6 transferred and absorbed by the cooling fluid. The middle flow channel domain, also named
 7 the design domain, is constituted by both fluid and solid (cubic) elements at a given void
 8 fraction (Φ), each element having $W_{element}$ in width and $L_{element}$ in length (Fig. 1b). Their spatial
 9 distribution determines consequently the topology of the flow path and the cooling performance
 10 that should be optimized. One special case is the conventional straight channel configuration,
 11 with a channel width of w_{ch} and a separating wall thickness of w_{sw} between two neighboring
 12 channels, which is shown in Figure 1 (a) and considered as the reference design (abbreviated
 13 as “RSC” hereafter) for performance comparison.

14



15

16 **Figure 1. Schematic view of the heat sink model for GATO. (a) A special case of a parallel straight channel**
 17 **heat sink (RSC) and (b) Design domain represented by fluid or solid (cubic) elements.**

1 The following assumptions and simplifications have been made for this study:

- 2 • Steady-state, in-compressible and Newtonian fluid flow;
- 3 • Negligible radiation heat transfer; negligible heat loss to the environment;
- 4 • No phase change for the working fluid.

5
6 Equations for mass and energy conservation could then be written as:

$$7 \quad \dot{m}_{in} = \dot{m}_{out} \quad (1)$$

$$8 \quad Q = \iint q \, dA_{design} = \dot{m}_{in}(Cp_{f,out}T_{f,out} - Cp_{f,in}T_{f,in}) \quad (2)$$

9 Where \dot{m}_{in} or \dot{m}_{out} is the inlet or outlet mass flow rate of the cooling fluid, respectively. Q is
10 the total input power; q is the heat flux at the heating surface; Cp_f is the specific heat of cooling
11 fluid; $T_{f,in}$ or $T_{f,out}$ is the inlet or outlet fluid temperature, respectively.

12 13 **2.2 GA procedure**

14 A GA procedure is developed to determine the best spatial distribution of the fluid and solid
15 elements in the design domain. The objective function is defined as the minimization of the
16 peak temperature of the heating surface (T_{peak}) (also called the fitness function in GA procedure)
17 under the constraint of constant void fraction (Φ) for the fully connected fluid phase. The reason
18 for this fully connected fluid domain constraint is to prevent the existence of isolated fluid
19 element(s) enclosed by solids, which may cause the boiling of fluid due to local overheating.
20 To do this, the design domain is gridded into r rows and c columns, and expressed by a binary
21 matrix $M_{(r \times c)}$. Each element in M represents either solid (0) or fluid (1) as shown in Fig. 1b.
22 the TO problem can then be formulated as Eq. (3).

23 Find $M_{(r \times c)}$

24 Minimize T_{peak}

25 s.t.

$$26 \quad \begin{cases} \Phi = constant \\ Connectivity = 1 \end{cases} \quad (3)$$

27
28 The general principle of GA is to assess the individuals among a starting random population,
29 keep the best ones that meet the objective function (or fitness), and then cross and mutate
30 them to get a new child population of the same size, and so on. One generation after another,
31 the best design is expected to be determined. The main procedure of GA in this study is shown
32 in the flow chart (Fig. 2) and described in detail below.

- 1 • **Initial generation:** a number of $M_{(r \times c)}$ matrices (100 in this study) are generated by
2 random allocation of 0 and 1 elements at a fixed Φ . The repeatability and connectivity
3 are checked to guarantee that only the non-repeated M with a fully connected fluid
4 domain is included. Each M is treated as an individual in this generation to be evaluated
5 in the next steps.
- 6 • **Geometry transformation:** all the matrices in the generation would be transformed
7 into real geometry models (such as shown in Fig. 3) by writing all the dimensions and
8 0 & 1 distribution information into a coded script as an executable file for the CFD tool.
- 9 • **Performance evaluation of individuals:** the fluid flow and heat transfer
10 characteristics of each configuration are calculated by the CFD method. Especially, the
11 objective function (T_{peak} in this study) values of individuals are obtained and extracted.
- 12 • **Ranking, selection, and elites keeping:** all the tested individuals are ranked
13 according to the fitness. A certain amount of well-evaluated configurations (50 in this
14 study, ranked from 2 to 51) with a higher ranking are selected as future parents to
15 create the individuals of the next generation while others are eliminated from
16 reproduction. Note that the top-ranked individual(s) are considered as the elite(s) (1 in
17 this study) and would be maintained in the next generation, preventing the loss of the
18 most fitted “genes” [40].
- 19 • **Crossover and Mutation:** Crossover operation is firstly performed on two neighboring
20 individuals from the top 2 to the top 51 on the ranking list (top one as elite) to produce
21 two children. One-point crossover is used in the current study [41], i.e., based on a
22 randomly selected element in the matrix either horizontal or vertical crossover is
23 performed with equal probability. Then, each produced child is set to have a 20%
24 probability to mutate, by either horizontal or vertical string swapping with equal
25 probability. In that way, better genes (regarding fitness) would be inherited while in the
26 meantime good diversity could be ensured. 100 children are generated and at the same
27 time, the constant void fraction and connectivity constraints are obeyed. Detailed
28 information about the crossover and mutation operations is given in Supplementary
29 Material S1 of this paper.
- 30 • **Dead ends elimination:** In case one fluid element is surrounded on three sides by
31 solid cells, the flow velocity is usually near zero thus the cooling effect at these ends
32 might be low. Therefore, an additional step is to eliminate these fluid elements,
33 considered dead ends, by randomly exchanging their locations with some solid cells,
34 keeping always the constant Φ and full connectivity. More explanation about this step
35 may be found in Supplementary Material S2. All the matrices in this new generation will

then be transferred to the geometry transformation step for recurrence following the above-explained procedure.

- **Termination criterion:** the GATO algorithm is considered to be completed when the variation of the median value of the objective function (T_{peak}) is smaller than 1×10^{-4} from one generation to the next for at least 10 generations (Eq. 4). The geometry and the thermo-hydraulic characteristics of the optimum topology will be exported.

$$\left| \frac{T_k^{median} - T_{k-1}^{median}}{T_{k-1}^{median}} \right| < 1 \times 10^{-4}; \left(\sum_{k=n-9}^n \left| \frac{T_k^{median} - T_{k-1}^{median}}{T_{k-1}^{median}} \right| \right) < 1 \times 10^{-3} \quad (4)$$

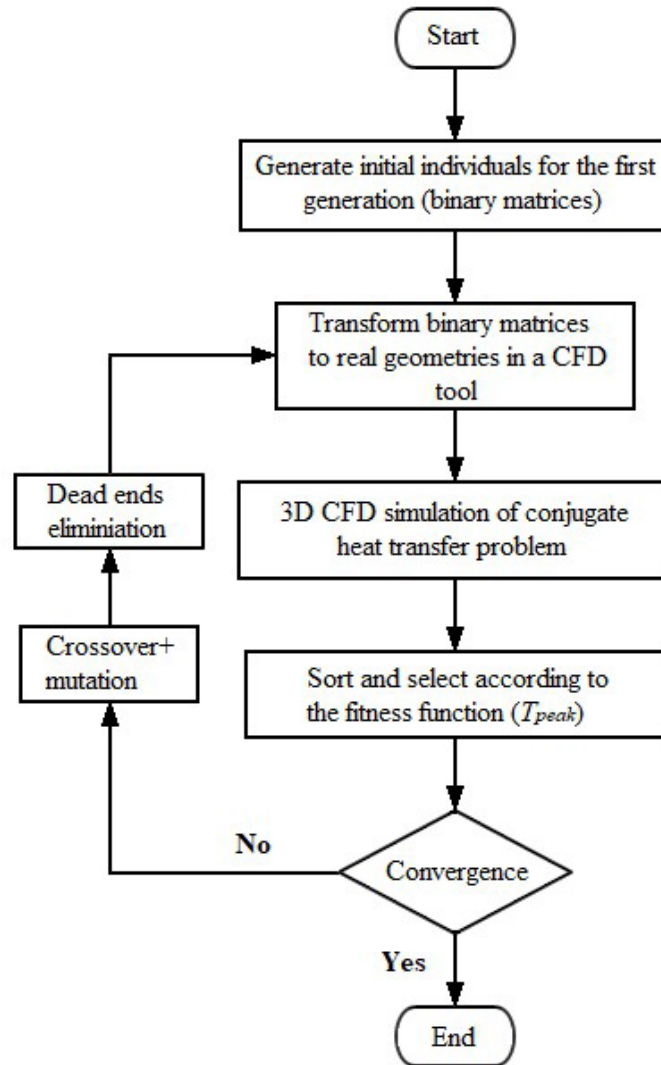


Figure 2. Flow chart of the GATO algorithm for global flow channel optimization in heat sinks

2.3 Calculation of flow and temperature fields by CFD method

The fluid flow and heat transfer characteristics of each flow channel configuration are calculated by CFD simulation. The governing equations under steady-state are shown as follows:

1 Continuity equation:

$$2 \quad \nabla \cdot (\rho \vec{v}) = 0 \quad (5)$$

3 Momentum conservation equation:

$$4 \quad \nabla \cdot (\rho \vec{v} \vec{v}) = -\nabla p + \nabla \cdot (\bar{\bar{\tau}}) + \rho \vec{g} + \vec{F} \quad (6)$$

5 Where p is the static pressure; $\bar{\bar{\tau}}$ is the stress tensor; $\rho \vec{g}$ and \vec{F} are the gravitational body force
6 and external body force.

7
8 Energy equation:

$$9 \quad \nabla \cdot (\vec{v}(\rho E + p)) = \nabla \cdot (\lambda_{eff} \nabla T - \sum_j H_j \vec{j}_j + (\bar{\bar{\tau}}_{eff} \cdot \vec{v})) \quad (7)$$

10 Where λ_{eff} is the effective conductivity; H is the sensible enthalpy; $\bar{\bar{\tau}}_{eff}$ is the effective shear
11 stress. For the solid zone, the energy transport equation is:

$$12 \quad \nabla \cdot (\lambda_s \nabla T) + S_{hs} = 0 \quad (8)$$

13 Where S_{hs} is the heat source within the solid. Detailed simulation parameters used in this study
14 are presented in section 3.1.

15 16 **2.4 Performance indicators and non-dimensional parameters**

17 Various parameters are used as performance indicators, introduced below. The global thermal
18 resistance of heat sink (R_{th}) is calculated as follows:

$$19 \quad R_{th} = \frac{T_{peak} - T_{in}}{Q} \text{ (K} \cdot \text{W}^{-1}\text{)} \quad (9)$$

20 Where T_{peak} is the maximum temperature at the heating surface (base wall) of the heat sink,
21 T_{in} is the inlet fluid temperature, and Q is the total input power.

22
23 The overall pressure drop of the heat sink is calculated as the pressure difference between the
24 inlet and outlet ports:

$$25 \quad \Delta P = P_{in} - P_{out} \quad (10)$$

26
27 The Nusselt number (Nu) of the heat sink and the Reynolds number (Re) at the inlet channel
28 are calculated by Eqs. (11) and (12), respectively:

$$29 \quad Nu = \frac{h_{avg} \cdot D_{h,design}}{\lambda_f} \quad (11)$$

$$30 \quad Re_{in} = \frac{\rho_f \cdot v_{in} \cdot D_{h,in}}{\mu_f} \quad (12)$$

1 Where λ_f , ρ_f and μ_f are the thermal conductivity, density, and dynamic viscosity of the fluid,
 2 respectively. v_{in} is the inlet flow velocity and $D_{h,in}$ is the hydraulic diameter of the inlet channel.
 3 The hydraulic diameter $D_{h,design}$ of the flow channels in the design domain is calculated as
 4 follows [42]:

$$D_{h,design} = \frac{4V_{ch}}{S_w} \quad (13)$$

6 Where V_{ch} and S_w are the total wetted volume and the total wetted surface area of the flow
 7 channels in the design domain, respectively. The average heat transfer coefficient h_{avg} is
 8 calculated by Eq. (14):

$$h_{avg} = \frac{Q}{A_{eff}(T_{w,avg} - T_{f,avg})} \quad (14)$$

10 Where A_{eff} is the effective solid-fluid interface area, $T_{w,avg}$ is the average channel wall
 11 temperature, and $T_{f,avg}$ is the average fluid temperature calculated by:

$$T_{f,avg} = \frac{T_{f,in} + T_{f,out}}{2} \quad (15)$$

13
 14 The standard deviation of temperature (STD_T) at the heating surface is calculated as:

$$STD_T = \sqrt{\frac{1}{n-1} \sum_{Pix=1}^n (T_{Pix} - \bar{T})^2} \quad (16)$$

16 Where n is the total number of points with temperature value at the heating surface; Pix is the
 17 No. Pix point and \bar{T} is the average temperature at the heating surface.

18
 19 Velocity, temperature, and pressure values are normalized as below:

$$v^* = \frac{v}{v_{in}} \quad (17)$$

$$T^* = \frac{T - T_{f,in}}{T_{f,out} - T_{f,in}} \quad (18)$$

$$P^* = \frac{P}{P_0} \quad (19)$$

23 Where P_0 is pressure drop when the design void fraction (Φ) is equal to 1.

24
 25

26 **3. Benchmark case and optimization results**

27 In this section, the optimization results of a benchmark heat sink case are presented to show
 28 the feasibility and effectiveness of the proposed GATO method.

29

3.1 Benchmark case and numerical parameters

Figure 3 shows the 3-D CFD model for the studied benchmark case of the heat sink subjected to GATO as well as the detailed dimensions. The middle design domain has a square shape of 50 mm × 50 mm, represented by a binary matrix of $M_{50 \times 50}$. The fluid void fraction (Φ) for this benchmark case is set as 0.50, i.e. equal number of solid and fluid elements, and their distribution is subjected to optimization. Recall that for the convenience of simulation and optimization, the entire fluidic circuit has an identical channel depth of $e=1$ mm, making every fluid or solid element as a cubic form to morph. The channel depth could also be a parameter for a real 3D TO of the fluid domain, but not considered in this study.

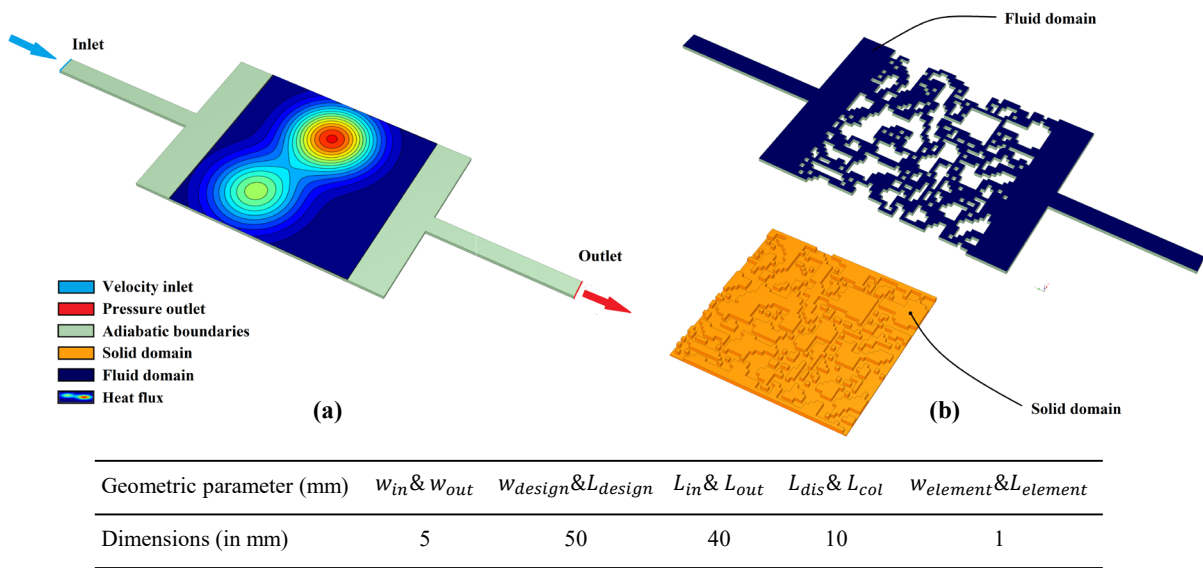


Figure 3. Heat sink geometry and dimensions for the benchmark study. (a) Geometry and boundary conditions; (b) example of solid and fluid domains

Water and aluminum are used as the fluid phase and the solid phase, respectively. Their physical properties are considered as constant, i.e., $\rho_f=998.2 \text{ kg} \cdot \text{m}^{-3}$; $\lambda_f=0.6 \text{ W} \cdot \text{m}^{-1} \cdot \text{K}^{-1}$; $C_{p,f}=4182 \text{ J} \cdot \text{kg}^{-1} \cdot \text{K}^{-1}$; $\mu=1.003 \times 10^{-3} \text{ Pa} \cdot \text{s}$ for fluid and $\rho_s=2719 \text{ kg} \cdot \text{m}^{-3}$; $\lambda_s=202.4 \text{ W} \cdot \text{m}^{-1} \cdot \text{K}^{-1}$; $C_{p,s}=871 \text{ J} \cdot \text{kg}^{-1} \cdot \text{K}^{-1}$ for solid.

3D CFD simulations were performed to calculate the fluid flow and heat transfer characteristics of each design. Fluid velocity inlet ($v_{in}=0.1 \text{ m} \cdot \text{s}^{-1}$) normal to the inlet boundary surface was set, with an inlet temperature of 293 K. The corresponding inlet Reynolds number Re_{in} was 166 to make sure the whole flow domain is under laminar regime. The pressure outlet boundary was set for the outlet surface with zero-gauge pressure. All walls were considered non-slip and adiabatic, except for the upper surface of the design domain (heating surface of the heat sink). For the latter, a Gaussian-shape two-peak heat flux distribution is defined, given by Eq. (20):

$$q(x, y) = \sum_{i=1}^2 B_i e^{-\frac{(x-x_i)^2+(y-y_i)^2}{2\sigma_i^2}} \quad (20)$$

The heat flux peak located at the position (x_i, y_i) has a maximum value of B_i , and σ_i indicates the spatial spread. The total power of the heat sources is equal to 90 W, corresponding to an average heat flux (power density) for the heating surface of $q_{avg} = 3.6 \text{ W}\cdot\text{cm}^{-2}$. Detailed values of parameters in Eq. (20) and the shape of the heat fluxes are given in Table 1.

Table 1. Gaussian-shape two-peak heat flux

| | x_i (mm) | y_i (mm) | B_i ($\text{W}\cdot\text{cm}^{-2}$) | σ_i (mm) | |
|-------------------|------------|------------|---|-----------------|--|
| Heat flux (HF) 1: | | | | | |
| 1 | 37.5 | 25 | 12.5 | 8.45 | |
| 2 | 12.5 | 33 | 9.5 | 8.45 | |
| Heat flux (HF) 2: | | | | | |
| 1 | 37.5 | 25 | 15.2 | 7.91 | |
| 2 | 12.5 | 33 | 9.5 | 7.91 | |
| Heat flux (HF) 3: | | | | | |
| 1 | 37.5 | 25 | 17.7 | 7.45 | |
| 2 | 12.5 | 33 | 9.5 | 7.45 | |

In this study, OpenFoam (version 7) was used to solve the governing equations (Eqs.10-13). Note that the gravity and viscous heating effects were not considered for simplification. The multi-physics conjugate heat transfer solver “chtMultiRegionFoam” in OpenFoam has been used for both solid and fluid domains [43]. No re-meshing is needed when updating the individuals from one generation to the next in the GATO procedure, thereby saving computational time and data storage. The laminar model was used for fluid flow due to the small Re numbers in the fluid domain. SIMPLE algorithm was employed for the velocity-pressure coupling. The solution was considered to be converged when (i) the maximum temperature of the heated surface and the inlet-outlet pressure drop were constant from one iteration to the next (less than 0.5% variation), and (ii) the normalized residuals were lower than 10^{-5} for the energy equation and 10^{-4} for other governing equations.

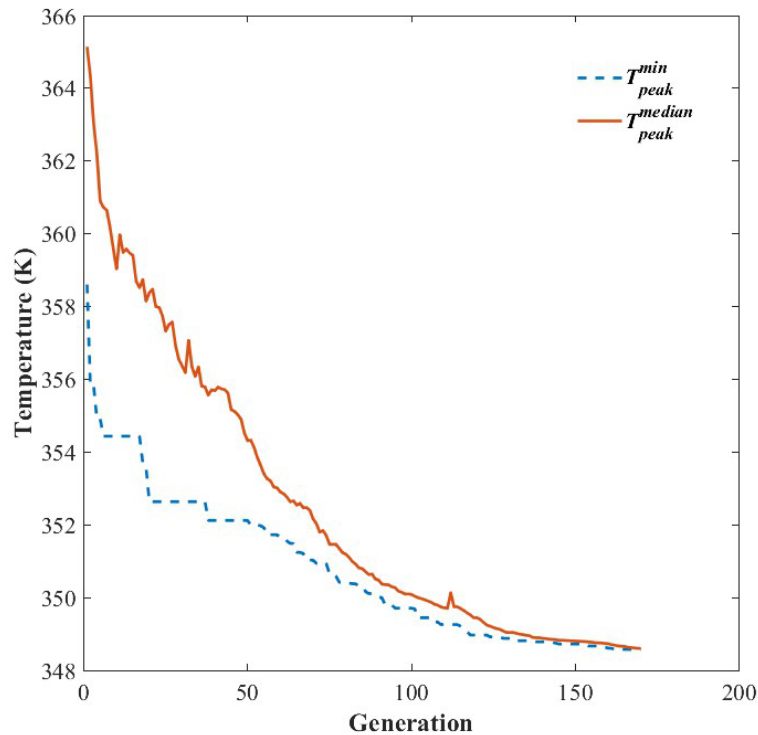
Structured cube shape meshes with equal edge lengths were generated. The grid used in the study had 129 k elements in total, with 71 k elements for the fluid zone and 56 k elements for

1 the solid zone. A grid independence study (on a randomly chosen individual in the initial
2 generation) was conducted to guarantee that the current mesh density used was appropriate
3 and sufficient regarding both accuracy and calculation time. More details of the mesh
4 independence study can be found in Supplementary Material S3 of this paper. The CFD
5 simulations using OpenFoam were performed with the help of a High-performance computing
6 (HPC) cluster CCIPL (Le Centre de Calcul Intensif des Pays de la Loire) [44]. Matlab (version:
7 R2020 a) was used for the matrix generation and updating, data processing, and GA procedure.

9 **3.2 Optimization results of the benchmark case**

10 Figure 4 depicts the evolution of T_{peak}^{min} and T_{peak}^{median} values amongst the 100 individuals along
11 with the increasing number of GA generations. More precisely, T_{peak}^{min} stands for the smallest
12 value of 100 T_{peak} in a generation while T_{peak}^{median} stands for the median value. It took 170
13 generations to meet the defined convergence criterion (Eq. 4), the value of T_{peak}^{median} being
14 decreased from 365.1 K to 348.6 K. Accordingly, the T_{peak}^{min} value also decreased continuously
15 from 358.6 K (generation 1) to 348.6 K (generation 170), indicating the effectiveness of the
16 proposed GATO method in attaining the defined optimization objective. Note that some stairs
17 appeared in the T_{peak}^{min} curve especially during the first half of the convergence, which is mainly
18 due to the elite keeping in GA: the crossover and mutation process cannot give birth to a better
19 individual that underscores the top-ranked one in the previous generation. Also note that at the
20 convergence, the T_{peak}^{min} and T_{peak}^{median} values are very close (but not the same), indicating that
21 the fitness difference between the top 50 individuals is very small.

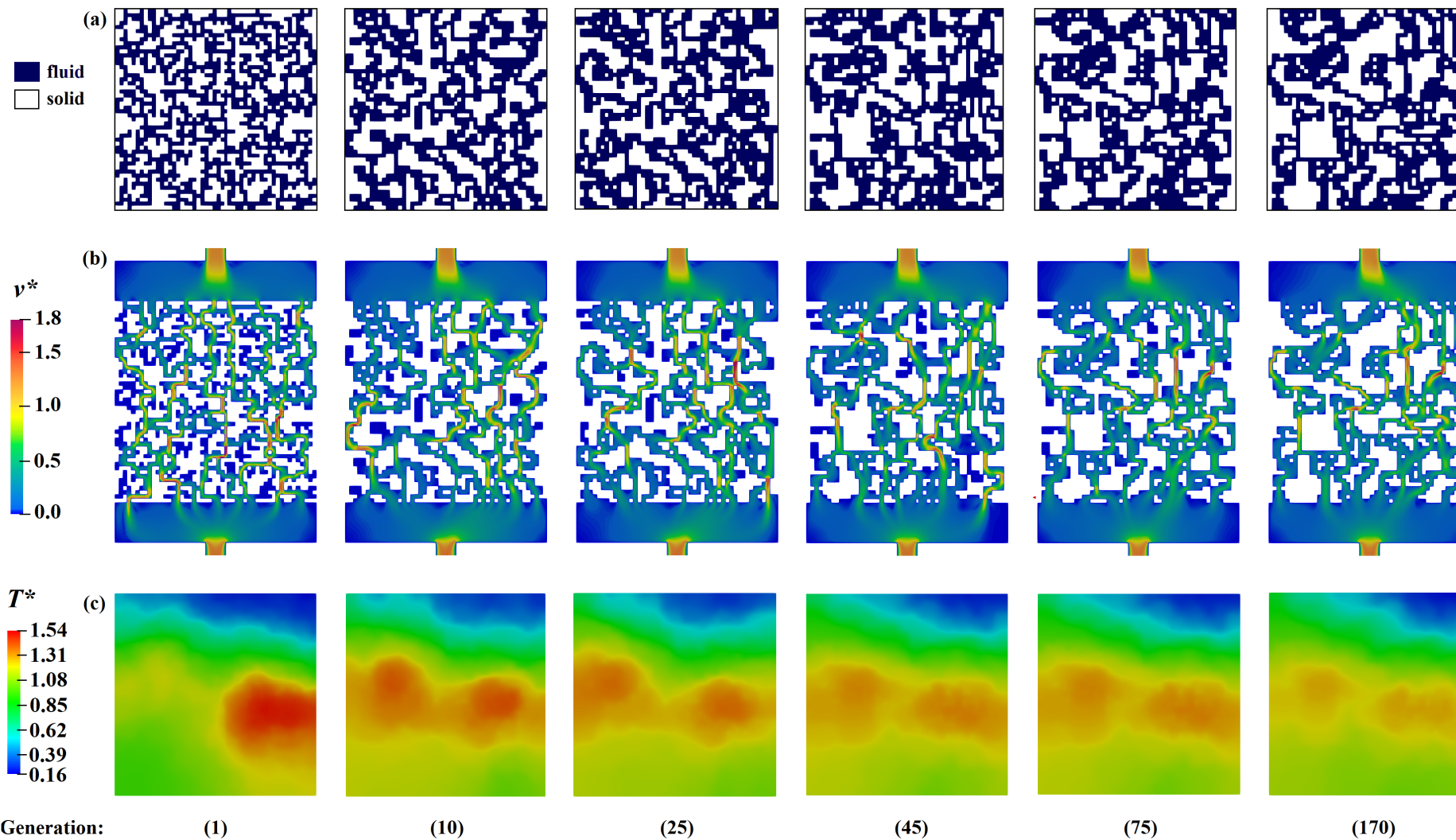
22
23 Figure 5 shows the flow channel configuration of the design domain (Fig. 5a), the
24 corresponding velocity fields (Fig. 5b) at the mid-plane of channel depth ($z^*=-0.5$), and the
25 temperature field (Fig. 5c) on the heating surface for the top-ranked individual of generation 1,
26 10, 25, 45, 74 and 170. It is clearly illustrated that the flow topology evolves during the GA
27 optimization to meet the objective function. In more detail, fluid elements tend to join together
28 and form larger channels near the inlet and outlet manifolds. In contrast, pin-fin structures and
29 small bifurcations and confluences are more likely to appear in the middle area where two heat
30 flux peaks are located. Such a trend increases the fluid-solid contacting surface area and
31 interrupts the formation of boundary layers, and enhances the cooling. The global structure of
32 the flow paths is more or less established at generation 45 (e.g., a big cluster of solid elements
33 downstream of the left heat flux peak) and inherited in the following generations. From then
34 on, local details (small transversal flow paths) are still generated and adjusted along with the
35 GA optimization.



1
2 **Figure 4. Evolution of T_{peak}^{min} and T_{peak}^{median} amongst the 100 individuals along with the increasing number of GA**
3 **generations**
4

5 At the end of generation 170, a higher proportion of cooling fluid is guided from the inlet to the
6 right part of the design domain. This is because the larger heat flux peak is located in this area
7 and closer to the outlet manifold, higher cooling capacity (higher mass and lower temperature
8 of coolant) is thereby needed to alleviate the temperature hot spots. The evolution of the
9 temperature field on the heating surface along with GA steps (Fig. 5c) shows clearly the better
10 cooling performance of the heat sink by optimization of the flow path topology. The temperature
11 hot spots gradually disappear and the isotherms become more parallel to the line connecting
12 the two hot spots. perpendicular to the global flow direction (from the inlet to the outlet) along
13 with better temperature uniformity.

14
15 The results of this benchmark case indicate that at the constraint of constant void fraction (Φ),
16 the fluid elements have been arranged more efficiently to form an adapted flow configuration
17 corresponding to the power and location of heat sources. In this way, the T_{peak} (objective) can
18 be decreased generation by generation by the GATO method, achieving the best convective
19 cooling of the heating surface with multiple-peak heat flux.
20



1

2

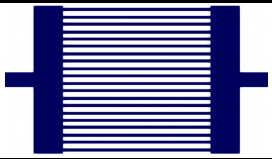
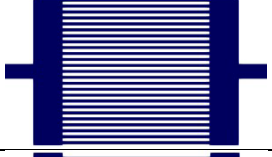
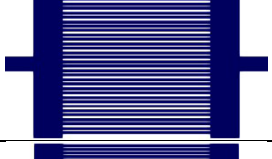
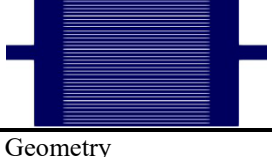
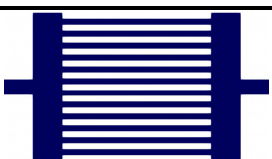
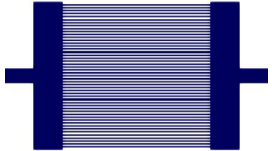
3

Figure 5. Top-ranked flow path configuration for the benchmark case at generation 1, 10, 25, 45, 74, and 170. (a) Fluid/solid elements distribution in the design domain; (b) Corresponding velocity field at mid-plane of channel depth ($z^* = -0.5$); (c) Temperature field at the heating surface

4. Effects of design variables of GATO on the optimized channel configuration: a parametric study

In section 3, the GATO has been successfully applied to obtain the optimal flow configuration (heat sink geometry) for the benchmark case. Here the optimized flow topology (named as GATO heat sink hereafter) as a function of the key design and operating variables is investigated, including the heat flux shape (HF), the void fraction (Φ), the inlet flow velocity (V_{in}), and the design domain resolution (M_{rxc}). Note that other parameters are kept the same as the benchmark except for the variable being evaluated. The conventional RCS heat sink as shown in Fig. 1a has also been introduced for testing. To make it comparable, the geometrical parameters of the RCS heat sinks may be different based on the various parameters we investigate in this section, as presented in Table 2. Their cooling performances under the same design variables and operating conditions are compared and reported in Table 3.

Table 2. Geometry and dimensions of the RCS heat sinks introduced for performance comparison with GATO heat sinks

| Void fraction (Φ) | | | Geometry |
|--------------------------|--------------------|------|--|
| 0.40 | w_{ch} (mm) | 1 |  |
| | w_{sw} (mm) | 1.5 | |
| | Number of channels | 20 | |
| 0.50 (Benchmark) | w_{ch} (mm) | 1 |  |
| | w_{sw} (mm) | 1 | |
| | Number of channels | 25 | |
| 0.65 | w_{ch} (mm) | 1 |  |
| | w_{sw} (mm) | 0.5 | |
| | Number of channels | 32 | |
| 0.80 | w_{ch} (mm) | 1 |  |
| | w_{sw} (mm) | 0.25 | |
| | Number of channels | 40 | |
| Matrix resolution | | | Geometry |
| $M_{25 \times 25}$ | w_{ch} (mm) | 2 |  |
| | w_{sw} (mm) | 1 | |
| | Number of channels | 12 | |
| $M_{100 \times 100}$ | w_{ch} (mm) | 0.5 |  |
| | w_{sw} (mm) | 0.5 | |
| | Number of channels | 50 | |

1

Table 3. Performance comparison between GATO and RSC heat sinks under different heat fluxes

| <i>Influence of peak heat flux shape</i> | | | | | | | | | | | |
|---|-----------|-----|--|------|-----------|------|-----------------------------|-------|----------------------------|------|--|
| Heat Flux | <i>Nu</i> | | <i>R_{th}</i> (K·W ⁻¹) | | <i>P*</i> | | <i>T_{peak}</i> (K) | | <i>STD_T</i> (K) | | |
| | GATO | RSC | GATO | RSC | GATO | RSC | GATO | RSC | GATO | RSC | |
| HF1 | 5.7 | 3.8 | 0.58 | 0.64 | 1.88 | 1.15 | 345.5 | 351.3 | 10.3 | 13.0 | |
| HF2 | 5.7 | 3.9 | 0.61 | 0.70 | 1.82 | 1.15 | 348.5 | 356.8 | 11.4 | 14.3 | |
| HF3 | 5.3 | 3.9 | 0.64 | 0.75 | 1.92 | 1.15 | 351.3 | 361.0 | 11.7 | 15.5 | |

| <i>Influence of fluid void fraction</i> | | | | | | | | | | | |
|--|-----------|-----|--|------|-----------|------|-----------------------------|-------|----------------------------|------|--|
| ϕ | <i>Nu</i> | | <i>R_{th}</i> (K·W ⁻¹) | | <i>P*</i> | | <i>T_{peak}</i> (K) | | <i>STD_T</i> (K) | | |
| | GATO | RSC | GATO | RSC | GATO | RSC | GATO | RSC | GATO | RSC | |
| 0.4 | 5.6 | 4.4 | 0.63 | 0.72 | 3.89 | 1.20 | 350.0 | 358.0 | 10.6 | 13.6 | |
| 0.5 | 5.7 | 3.9 | 0.61 | 0.70 | 1.82 | 1.15 | 348.5 | 356.8 | 11.4 | 14.3 | |
| 0.65 | 5.3 | 3.3 | 0.59 | 0.71 | 1.30 | 1.10 | 346.4 | 357.3 | 12.9 | 15.5 | |
| 0.8 | 5.6 | 2.1 | 0.59 | 0.70 | 1.13 | 1.08 | 346.8 | 356.2 | 13.7 | 16.3 | |

| <i>Influence of inlet velocity</i> | | | | | | | | | | | |
|--|-----------|-----|--|------|-----------|------|-----------------------------|-------|----------------------------|------|--|
| <i>V_{in}</i> (<i>Re_{in}</i>) | <i>Nu</i> | | <i>R_{th}</i> (K·W ⁻¹) | | <i>P*</i> | | <i>T_{peak}</i> (K) | | <i>STD_T</i> (K) | | |
| | GATO | RSC | GATO | RSC | GATO | RSC | GATO | RSC | GATO | RSC | |
| 0.1 m·s ⁻¹ (166) | 5.7 | 3.9 | 0.61 | 0.70 | 1.82 | 1.15 | 348.5 | 356.8 | 11.4 | 14.3 | |
| 0.2 m·s ⁻¹ (332) | 7.8 | 5.1 | 0.40 | 0.48 | 2.09 | 1.14 | 329.7 | 336.3 | 6.9 | 9.2 | |
| 0.4 m·s ⁻¹ (663) | 10.6 | 5.9 | 0.31 | 0.36 | 4.21 | 1.12 | 321.5 | 326.1 | 5.8 | 6.7 | |

| <i>Influence of design domain resolution</i> | | | | | | | | | | | |
|---|-----------|-----|--|------|-----------|------|-----------------------------|-------|----------------------------|------|--|
| <i>Matrix resolution</i> | <i>Nu</i> | | <i>R_{th}</i> (K·W ⁻¹) | | <i>P*</i> | | <i>T_{peak}</i> (K) | | <i>STD_T</i> (K) | | |
| | GATO | RSC | GATO | RSC | GATO | RSC | GATO | RSC | GATO | RSC | |
| <i>M_{25×25}</i> | 7.8 | 5.3 | 0.69 | 0.87 | 1.30 | 1.10 | 356.1 | 372.1 | 12.1 | 15.0 | |
| <i>M_{50×50}</i> | 5.7 | 3.9 | 0.61 | 0.70 | 1.82 | 1.15 | 348.5 | 356.8 | 11.4 | 14.3 | |
| <i>M_{100×100}</i> | 4.9 | 1.7 | 0.53 | 0.63 | 2.33 | 1.34 | 341.3 | 350.6 | 12.6 | 15.2 | |

2

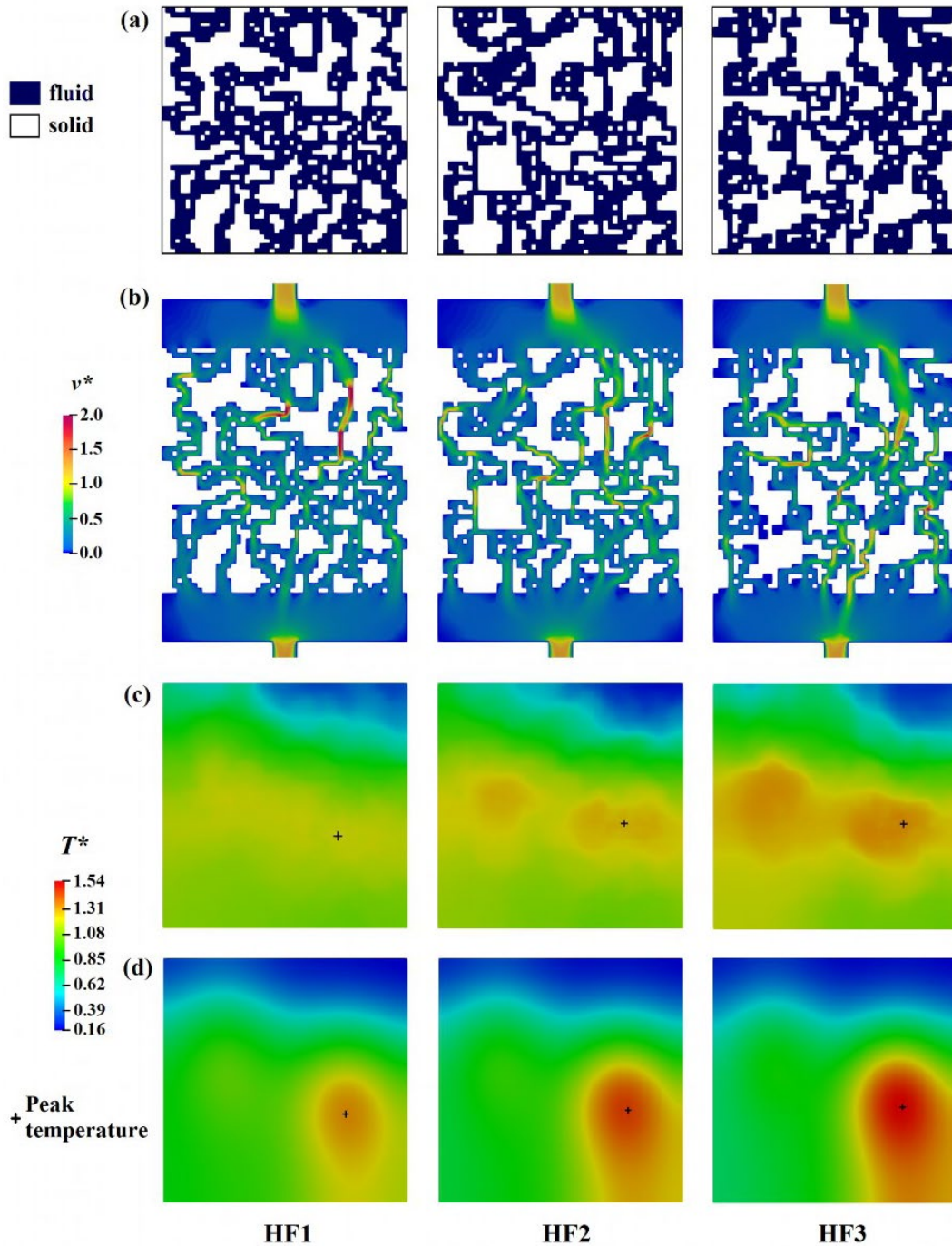
3 **4.1 Influences of peak heat flux shape**

4 Three heat fluxes shown in Table 1 have been used as input for the heating surface. They
5 have the same total power ($Q=90$ W; $q_{avg} = 3.6$ W·m⁻²) but differentiate between them by the
6 increasing value of the higher heat flux peak. The GATO has been executed for each and the
7 obtained optimization results are reported and discussed in this sub-section.

8

9 Shown in Figs. 6a and 6b are the optimal channel configurations of the design domain, and
10 the normalized velocity field, respectively. A similar general pattern may be observed, i.e.,

1 more fractionated small solid islands at the location of two heat flux peaks while bigger solid
 2 blocks in other regions. The more difference between the two peak values of the heat flux (e.g.,
 3 heat flux 3 (HF 3)), the more fluid elements are allocated at the right part of the design domain
 4 to deliver more mass of the cooling fluid to the higher temperature hot spot (cf. Fig. 6b).
 5



6
 7 **Figure 6. Influence of heat flux shape on the performance of GATO and RSC heat sinks. (a) optimized flow**
 8 **channel configuration by GATO; (b) velocity field ($z^* = -0.5$) of the GATO heat sink; (c) temperature field at the**
 9 **heating surface of the GATO heat sink; (d) temperature field at the heating surface of the RSC heat sink.**
 10

1 The temperature contours at the heating surface of GATO and RSC heat sinks are shown in
2 Figs. 6c and 6d, respectively. Temperature hot spots can be observed for the RSC heat sink,
3 while they are by and large eliminated (with clearly improved temperature uniformity) by the
4 optimized flow topology in the GATO heat sink. The T_{peak} value for the GATO heat sink is 345.5
5 K (HF 1), 348.5 K (HF 2), and 351.3 K (HF 3), respectively, smaller than that of the RSC heat
6 sink (351.3 K, 356.8 K, and 361.0 K, respectively). The greater the difference between two
7 peaks (e.g., HF 3), the more reduction of T_{peak} could be achieved by GATO compared to RSC.
8 The comparative results indicate clearly the fact that for highly heterogeneous heating surfaces,
9 the RSC as a basic (conventional) configuration becomes less performant. The necessity and
10 significant benefits of the GATO method are therefore highlighted.

11
12 Table 3 lists the performance indicators of GATO and RSC heat sinks subjected to different
13 heat fluxes. Generally, the Nu number of the GATO heat sink is about 40% - 50% higher than
14 that of the RSC heat sink, owing to the complex flow path configuration obtained that breaks
15 the thermal boundary layer of fluid and therefore enhances the convection heat transfer.
16 Nevertheless, the pressure drop is inevitably boosted due to the geometry complexity, and the
17 P^* value of GATO is clearly higher than that of RSC, However, the global pressure drop of the
18 GATO heat sink (< 220 Pa) is still small at this low flow rate condition. The R_{th} values follow
19 the same tendency as T_{peak} discussed above. The values of STD_T increase with the rising
20 difference of two heat flux peaks, but the temperature distribution is more uniform at the heating
21 surface of the GATO heat sink than that of the RSC heat sink.

22 23 **4.2 Void fraction (Φ) of the design domain**

24 The influence of void fraction on the cooling performance of the GATO heat sink has been
25 evaluated, by varying the Φ value from 0.40 to 0.80. The obtained results (optimized flow
26 channel configuration, velocity field, and temperature contours) are depicted in Figure 7.

27
28 At a low void fraction ($\Phi=0.4$), the limited amount of fluid elements is organized by GATO into
29 a flow circuit with relatively clear splitting or merging junctions. Fluid with higher velocity is
30 guided by the main flow paths to alleviate the temperature hot spots. In contrast, at a high void
31 fraction ($\Phi=0.8$), the excessive fluid elements are arranged like a porous medium where the
32 flow velocity is much lower. The numerous small solid islands work as pin-fin structures
33 surrounded by the cooling fluid calmly flowing, the contacting surface area is thereby higher.
34 Note from Fig. 7b that some fluid elements have near-zero velocity, implying that the void
35 fraction is not all efficiently used. The sharpening of the flow path could be done by eliminating
36 these fluid elements considered as dead volume, which will be further presented in section 5.1.

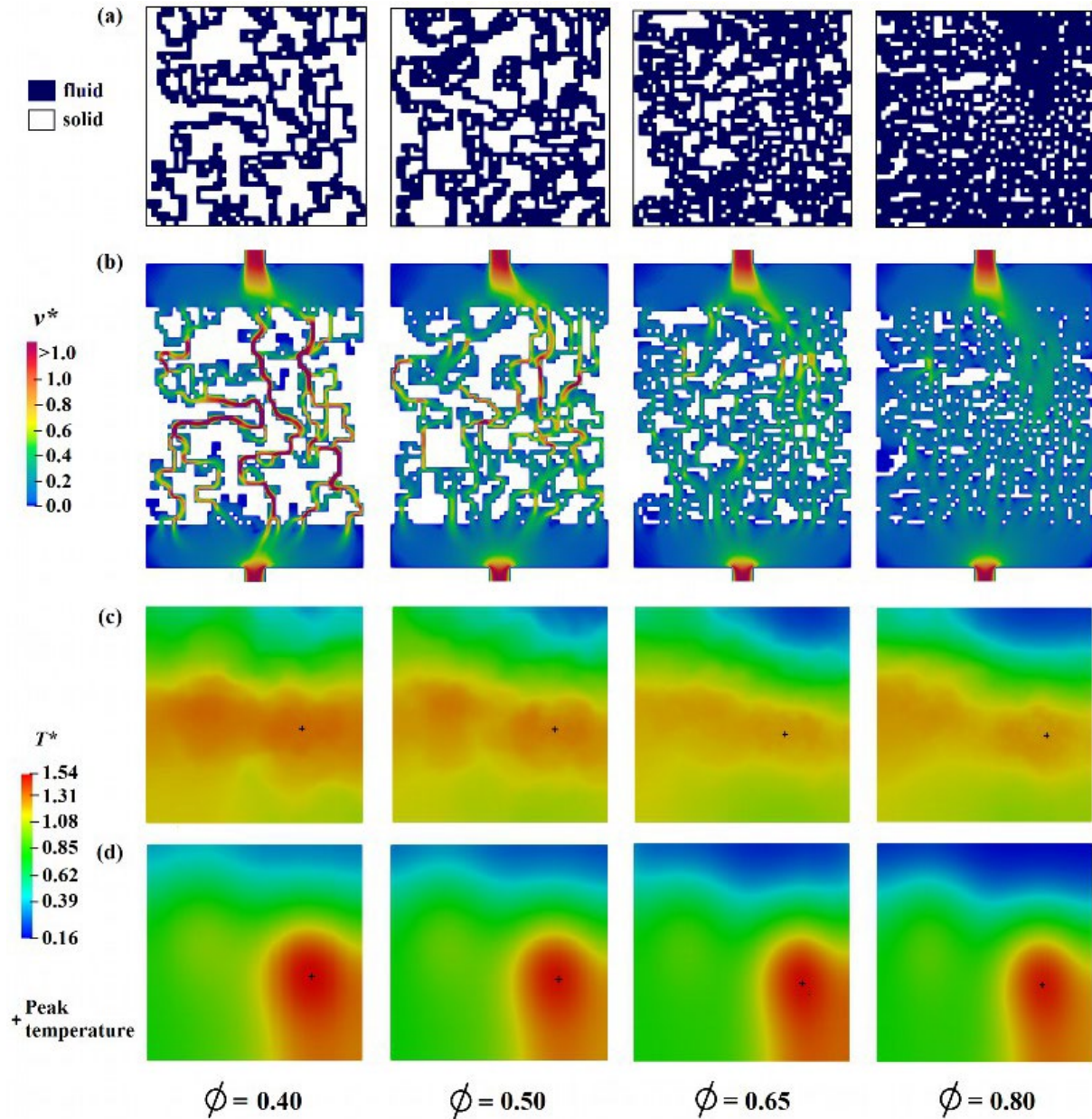


Figure 7. Influence of fluid void fraction (Φ) on the performance of GATO and RSC heat sinks. (a) optimized flow channel configuration; (b) velocity field ($z^*=-0.5$) of the GATO heat sink; (c) temperature field at the heating surface of the GATO heat sink; (d) temperature field at the heating surface of the RSC heat sink

By examining Fig. 7c, it is worth noting that the lowest T_{peak} value (346.4 K) is reached at $\Phi=0.65$ after GATO optimization. Higher or lower values of Φ render higher T_{peak} of the GATO heat sink, and also the higher R_{th} values as reported in Table 3. Such tendency still holds when the full range of Φ values is considered, with two extreme conditions $\Phi=0$ (no flow circuit) and $\Phi=1$ (cavity-type heat sink), clearly none of them is optimal in terms of cooling performance. Recall that Φ is treated as a constraint in the algorithm, i.e., constant Φ of all the individuals to be evaluated in the GATO. Such constraints may need to be revisited to achieve a more general optimum.

1 The performance comparison between the GATO and RSC heat sinks at different Φ values is
2 presented in Figs. 7c and 7d, and in Table 3 as well. The Nu numbers of GATO heat sinks are
3 very close, but all higher than those of RSC heat sinks with the same Φ , indicating better global
4 cooling performance. Regarding the RSC heat sink, the Nu number significantly decreases
5 with the increasing Φ . This is mainly due to an increase of the effective heat transfer surface
6 area A_{eff} (higher number of channels as shown in Table 2) between fluid and solid. Under the
7 same input power Q , the average heat transfer coefficient h_{avg} is therefore lowered. Moreover,
8 STD_T values for both GATO and RSC are larger at a high Φ value, this is because of the larger
9 low-temperature region at the entrance of the design domain, closer to the fluid inlet
10 temperature. But for the same Φ value, the GATO heat sink shows a more uniform temperature
11 distribution at the heating surface than that of the RSC heat sink, owing to the dispersed hot
12 spots by the optimized flow channel configuration.

13
14 The pressure drop of the GATO heat sink significantly increases with the decreasing Φ value,
15 i.e., P^* reaches 3.89 (429.4 Pa) at $\Phi=0.4$. Besides the higher velocity magnitude in the main
16 flow paths, the numerous splitting/merging junctions also create additional singular losses [45].
17 Regarding the RSC, the ΔP increase is relatively small, i.e., P^* ranging from 1.08 to 1.20.

18 19 **4.3 Inlet velocity**

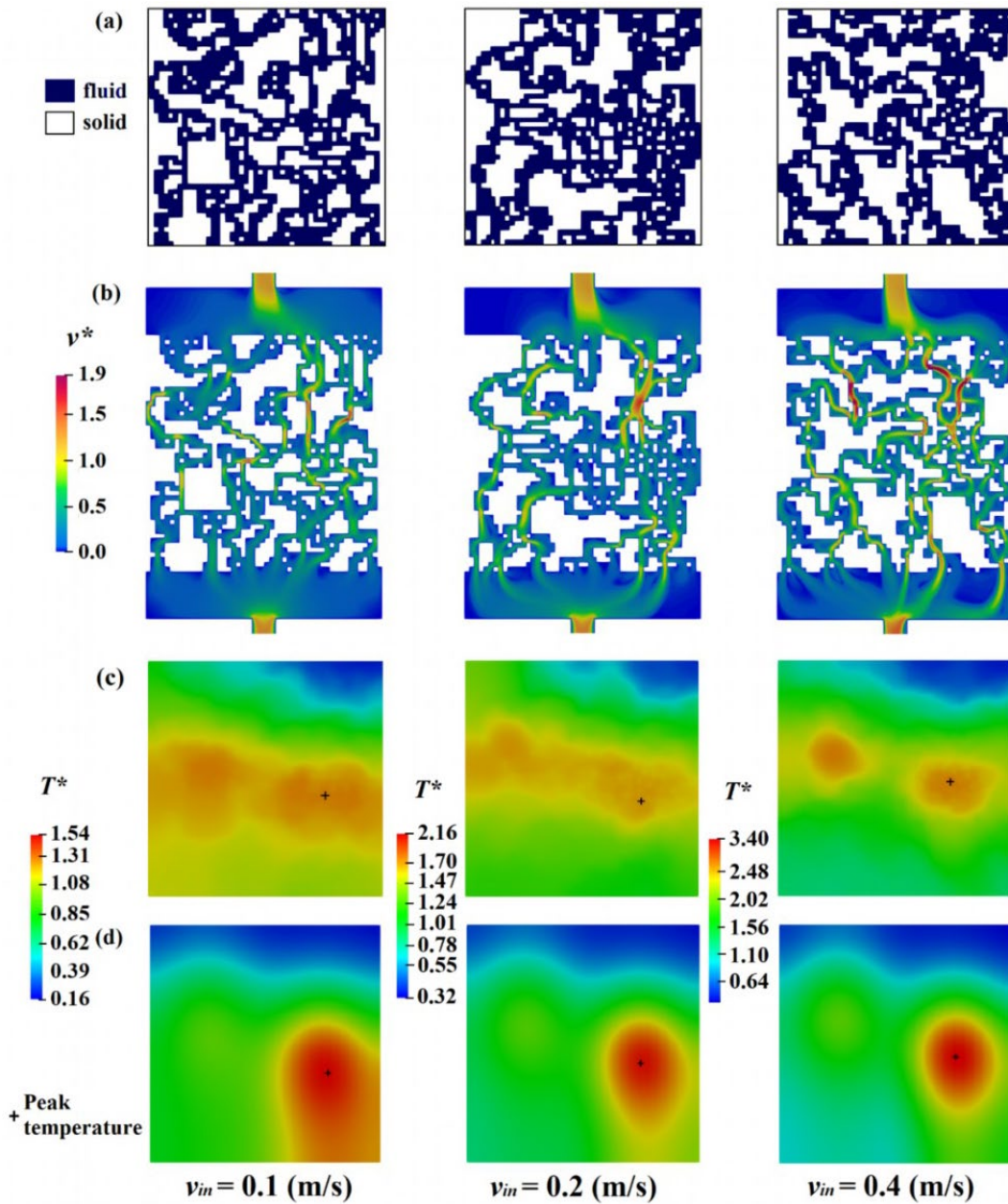
20 The benchmark heat sink has been optimized by GATO under different inlet velocities ($v_{in}=0.1$,
21 0.2 , and $0.4 \text{ m}\cdot\text{s}^{-1}$) to investigate the influence of increasing fluid flow rate (or Re_{in}) on the
22 optimized flow path configuration and its cooling performance. The optimization results as well
23 as the performance comparison with the RSC heat sink are reported in Fig. 8 and Table 3.

24
25 It can be observed from Figs. 8a and 8b that for all three tested inlet velocities, the main mass
26 flow is delivered to the position of heat flux peaks, and more fluid flow is guided towards the
27 higher peak than the smaller heat flux peak. When v_{in} increases, the main flow structure in the
28 entrance manifold tends to be fractioned into more small streams to compensate the stronger
29 inertial effect. Lower T_{peak} can be reached at a high v_{in} due to the higher cooling capacity, i.e.,
30 348.5 K ($v_{in}=0.1 \text{ m}\cdot\text{s}^{-1}$), 329.7 K ($v_{in}=0.2 \text{ m}\cdot\text{s}^{-1}$) and 321.5 K ($v_{in}=0.4 \text{ m}\cdot\text{s}^{-1}$), respectively.
31 Nevertheless, the normalized value T_{peak}^* (Eq. 18) increases with the increasing v_{in} due to the
32 smaller $(T_{f,out} - T_{f,in})$.

33
34 Table 3 lists the global thermal and hydraulic performances of GATO and RSC under different
35 v_{in} values for comparison. The increasing v_{in} (Re_{in}) results in the reduced R_{th} , T_{peak} , and STD_T
36 but the increased Nu and P^* . The higher cooling capacity at a high fluid mass flow rate

1 enhances the convection heat transfer. The augmentation of Nu number by applying the GATO
 2 method (compared to RSC heat sink) is more significant at a high flow rate, i.e., 46% at $v_{in}=0.1$
 3 $m \cdot s^{-1}$ whereas 80% at $v_{in}=0.4 m \cdot s^{-1}$. Furthermore, the GATO heat sinks optimized under three
 4 v_{in} values show better temperature uniformity than the corresponding RSC heat sinks. But with
 5 the increase of v_{in} , the difference in temperature uniformity tends to be smaller. This cooling
 6 performance enhancement is achieved at the cost of higher pressure drop (pumping power
 7 consumption) since in the current optimization algorithm, no hydraulic criterion is considered
 8 in the objective function nor as constraints.

9



10

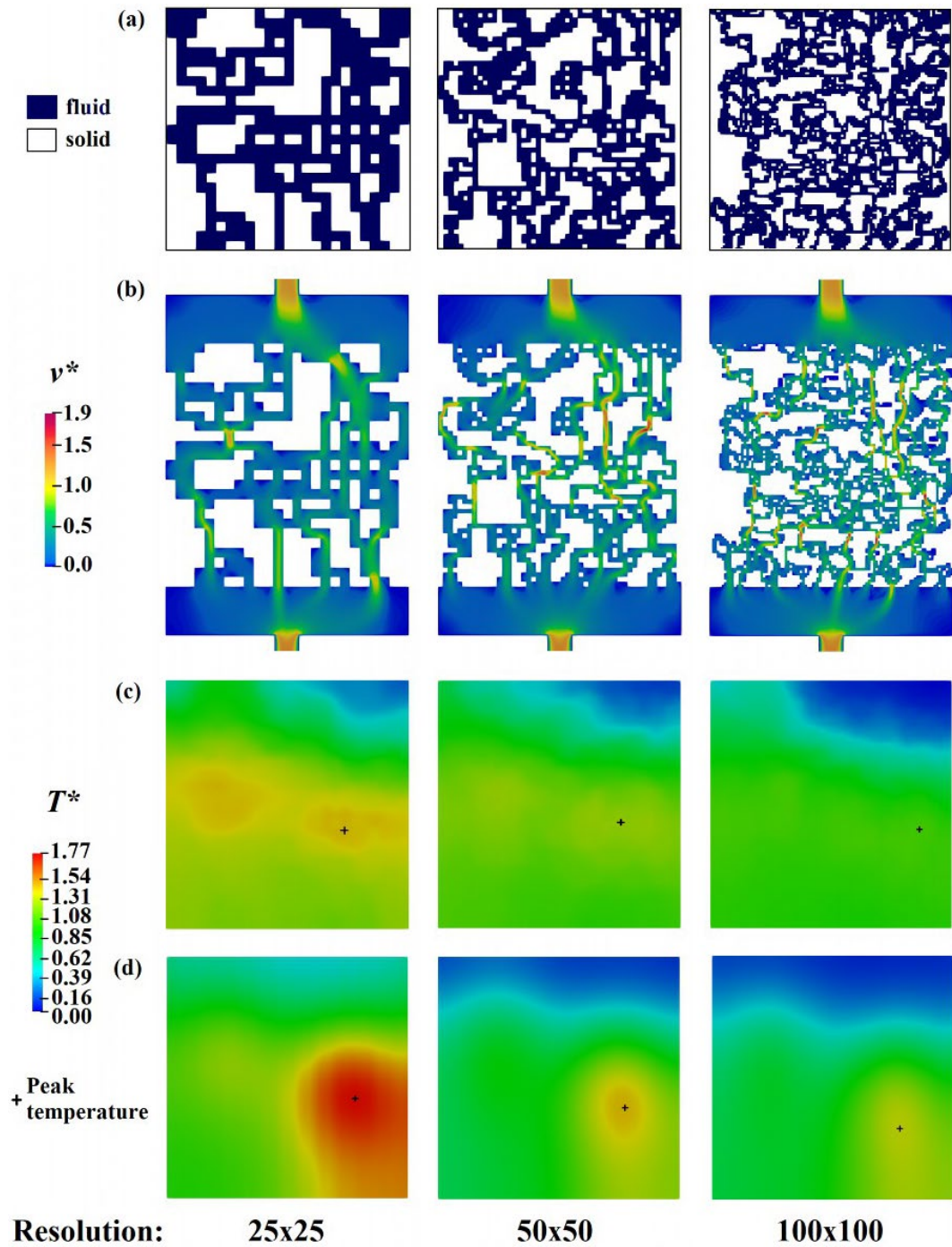
11 **Figure 8. Influence of inlet fluid velocity (v_{in}) on the performance of GATO and RSC heat sinks. (a) optimized**
 12 **flow channel configuration; (b) velocity field ($z^*=-0.5$) of the GATO heat sink; (c) temperature field at the**
 13 **heating surface of the GATO heat sink; (d) temperature field at the heating surface of the RSC heat sink.**

4.4 Design domain resolution

The design domain resolution ($M_{r \times c}$) determines directly the number of fluid and solid elements that can be allocated during the GA, thereby playing an important role in the optimization. To explore the influence of this structure fineness, the GATO has been executed under different matrix resolutions ($M_{25 \times 25}$, $M_{50 \times 50}$ and $M_{100 \times 100}$), other parameters being the same as the benchmark case ($\Phi=0.50$; $v_{in}=0.1 \text{ m}\cdot\text{s}^{-1}$; HF2). The optimization results are shown in Fig. 9.

Although a similar pattern of mass flow delivery at the global level is proposed by GATO, the flow path details are rather different at the local level. More local complex structures can be formed at the higher matrix resolution as shown in Figs. 9a and 9b. The higher number of elements to morph brings highly diversified individuals during the GATO optimization, capable of constructing thin and dense channels with split and recombine flow paths. Moreover, the solid-fluid interface area could be largely increased, leading to the lowered T_{peak} of the optimized flow channel configuration, i.e., 356.1 K at $M_{25 \times 25}$ and 341.3 K at $M_{100 \times 100}$.

Table 3 also presents the influence of $M_{r \times c}$ on the global thermal and hydraulic performances of the GATO heat sink. RSC heat sinks with the channel width equaling the element width ($w_{ch}=w_{element}$, cf. Fig. 1) are also introduced for comparison. Again, both the Nu number and the P^* of the GATO heat sink are higher than those of the RSC heat sink due to the above-explained reasons. Nu number for both types of heat sinks gradually declines with the increasing design resolution. This is because of the smaller hydraulic diameter (D_h) of the flow circuit on one hand, and the lowered h_{avg} on the other hand. In particular, the relatively small Nu number of RSC at $M_{100 \times 100}$ ($w_{ch}=0.5 \text{ mm}$) could be due to the strong heat conduction over the heat convection at small channel width [46]. The temperature distribution at the heating surface is the most uniform at $w_{ch}=1 \text{ mm}$ and $M_{50 \times 50}$ for both RSC and GATO heat sinks. Further increasing the mesh resolution (smaller channel size) will reduce the temperature uniformity due to the existence of a low-temperature region at the entrance of the design domain, as mentioned above. Higher pressure drop is also resulted at high $M_{r \times c}$, mainly due to the increased flow path complexity (thereby more singular losses). Moreover, a higher number of GA generations is needed to reach the convergence due to the increased number of design variables and the individual diversity, requiring more calculation time. Once optimized, the obtained flow circuit complexity with fine structures also put place higher demands on the level of manufacturing precision for its realization. Therefore, in practice, the appropriate design resolution should be decided by considering both the available computing resources and the fabrication capacity.



1
2 **Figure 9.** Influence of matrix resolution (M_{rxc}) on the performance of GATO and RSC heat sinks. (a) optimized
3 flow channel configuration; (b) velocity field ($z^*=-0.5$) of the GATO heat sink; (c) temperature field at the
4 heating surface of the GATO heat sink; (d) temperature field at the heating surface of the RSC heat sink
5
6

7 **5. Further discussions**

8 Further discussions are made on some issues raised above, to reveal and revisit the
9 effectiveness as well as the limitations of the proposed GATO method.
10

5.1 Post-treatment for dead volume elimination

Despite the dead-end elimination step in the optimization algorithm (cf. section 2.2), fluid elements with low-velocity magnitude are still numerous in the optimized GATO flow configuration, especially at a high void fraction (cf. Fig. 7). These fluid elements bring about unclear and ineffective fluid paths, which could be further removed by a post-treatment of the optimized flow topology. As an example, a threshold value of $v_{threshold}^* = 0.055$ has been applied for this purpose, i.e., all fluid elements having a velocity magnitude smaller than 5.5% of v_{in} are considered as dead volume and thus will be replaced by solid elements. The flow path configuration and the velocity field at different Φ values before and after this post-treatment are shown in Fig. 10.

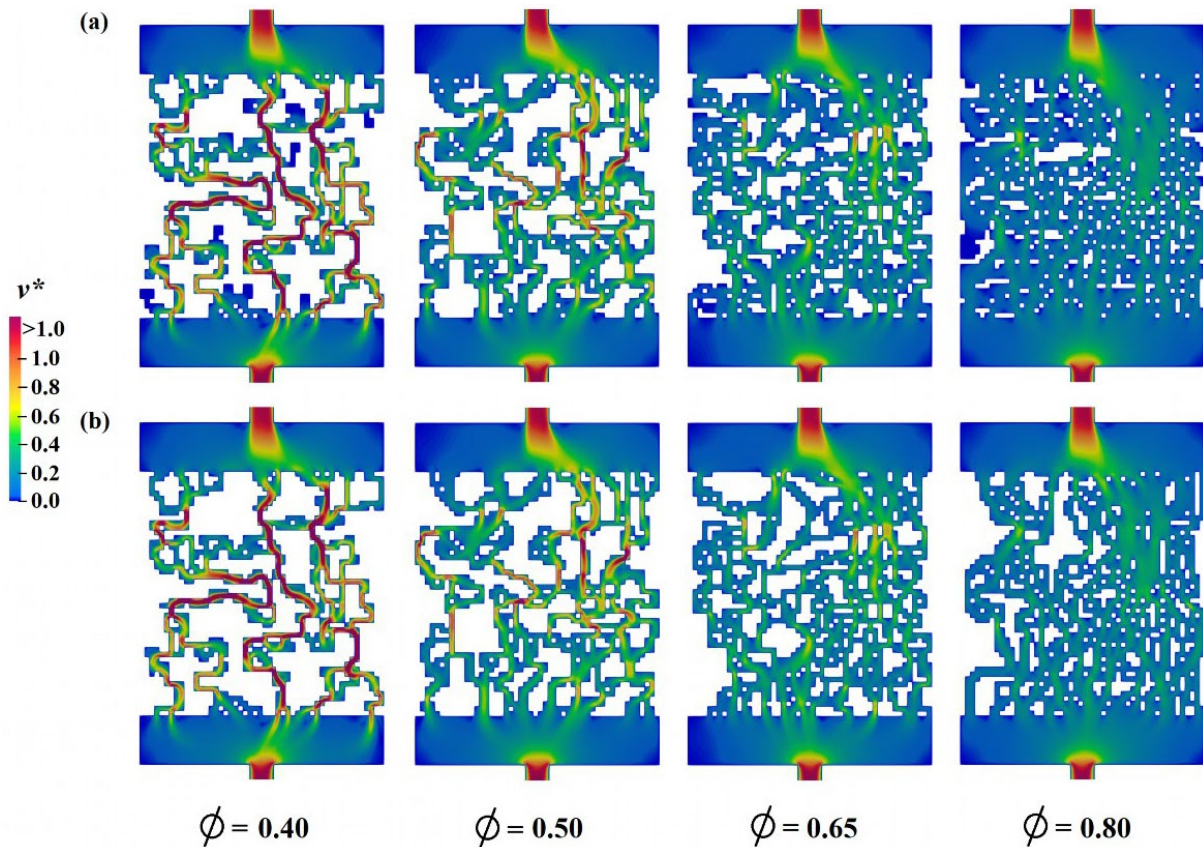


Figure 10. Post-treatment of the optimal flow configuration for dead volume elimination. (a) original optimized flow circuit; (b) flow circuit after post-treatment

It can be observed that the fluid paths become clearer, beneficial for the actual fabrication of the optimized heat sinks in practice. The effective void fraction (Φ) declines after post-treatment but has a negligible impact on the thermal and hydraulic performances of the heat sink (Table 4). Note that a higher threshold value may result in smoother flow structures, but this aspect has not been further explored in this study.

Table 4. Φ , T^* and P^* of the GATO heat sink before and after post-treatment for dead volume elimination

| Φ (before) | Φ (after) | T^* (before) | T^* (after) | P^* (before) | P^* (after) |
|-----------------|----------------|----------------|---------------|----------------|---------------|
| 0.40 | 0.36 | 1.31 | 1.31 | 3.89 | 3.90 |
| 0.50 | 0.44 | 1.28 | 1.27 | 1.82 | 1.84 |
| 0.65 | 0.56 | 1.22 | 1.22 | 1.30 | 1.32 |
| 0.80 | 0.65 | 1.24 | 1.24 | 1.13 | 1.16 |

5.2 Repeatability

The optimization algorithm has been executed two more times with the same settings for the benchmark case (cf. section 3.1), to test the reproducibility of flow configuration at convergence. The convergence curves are shown in Fig. 11. It can be observed that the T_{peak}^{median} values of the three runs at the convergence are very close (348.5 K, 348.9 K, and 349.3 K), with only a 1.26% difference. The final T_{peak}^{min} values are also quite close with a difference smaller than 0.7% (348.6 K, 348.8 K, and 349.0 K), indicating the good reproducibility of the GATO method in achieving the defined optimization objective. This difference should still be reduced by setting a more stringent convergence criterion (Eq. 4) but will be rather time-consuming due to the GA's nature.

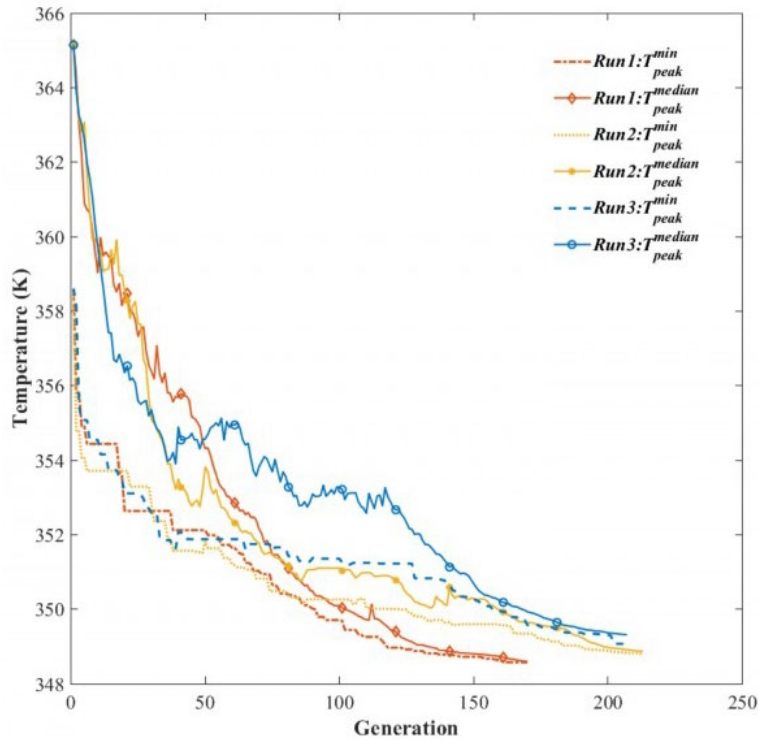
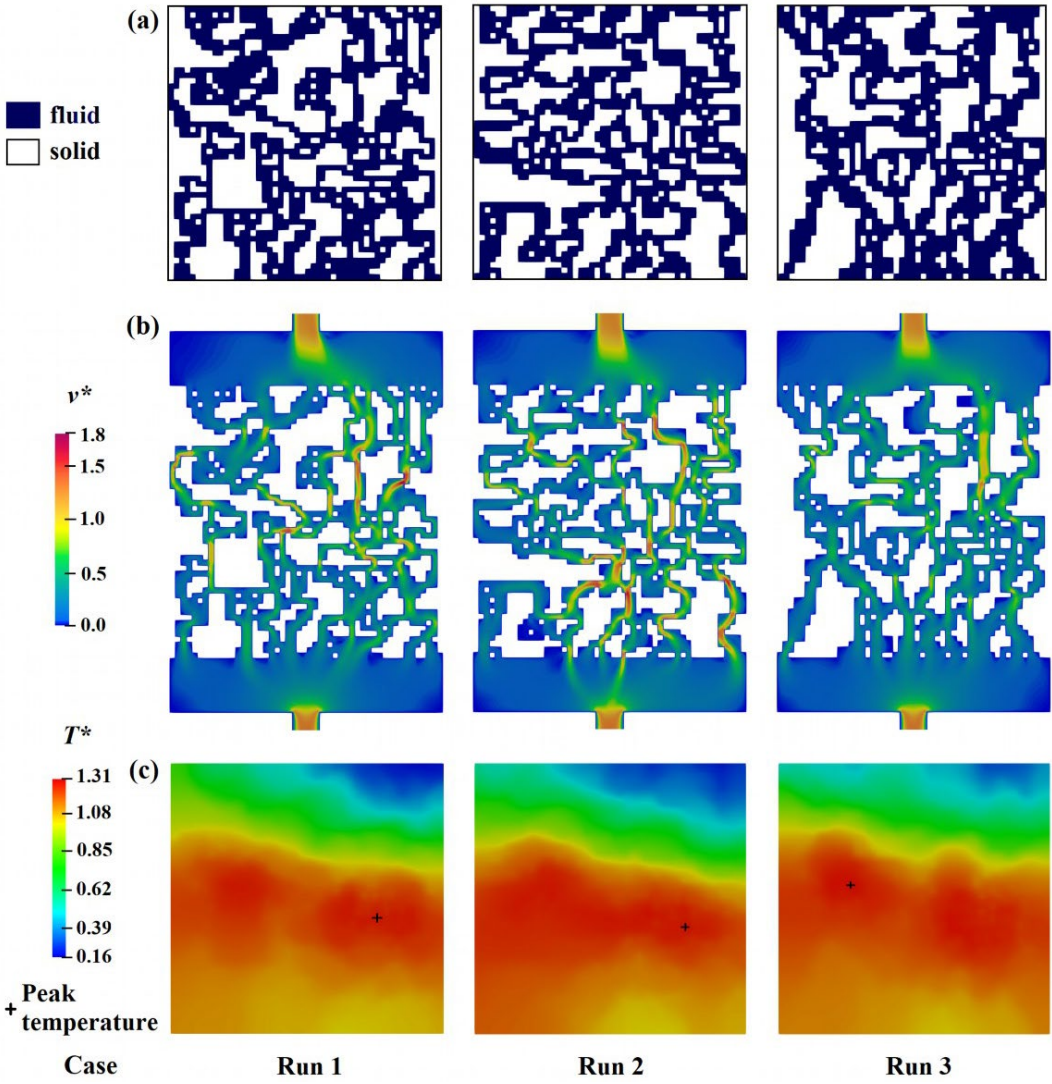


Figure 11. The convergence curve of T_{peak}^{median} and T_{peak}^{min} for three runs of the GATO method for the benchmark case

1 Nevertheless, a diversified optimized flow configuration has been obtained each time by
 2 running the GATO (Fig. 12), indicating the random feature during the crossover and mutation
 3 steps of the GA. They all provide the same cooling performance, i.e., the objective function
 4 (T_{peak}) is rather flat near the global optimal point regarding the variation of the fluid/solid
 5 elements distributions. This indicates that several solutions may be considered as very close
 6 to the global optimum, thus being good candidates in actual engineering practice.

7
 8 Figure 12c compares the temperature contour on the heating surface obtained by three runs
 9 of GATO. While the global pattern is quite similar (a small angle between isotherms and global
 10 flow direction due to the heat flux peak asymmetry), a slight difference at the local level can
 11 still be observed, especially regarding the position of the T_{peak} .

12



13 Case Run 1 Run 2 Run 3
 14 Figure 12. Comparison of the three runs of the GATO method for the benchmark case. (a) optimized flow
 15 configuration; (b) velocity field ($z^*=-0.5$); (c) temperature field at the heating surface
 16

1 **5.3 Simplifications made in CFD simulation**

2 Simplifications have been made in the CFD simulation to save the computational time,
3 including the negligible gravity and viscous heating effects (eligible for small channel depth
4 and small total ΔP), negligible heat loss to the ambient, and the temperature-independent
5 physical properties for both fluid and solid phases. In reality, the fluid viscosity could vary within
6 the operation temperature range, i.e., from $\mu = 1 \times 10^{-3}$ Pa·s at 293.15 K to 3.54×10^{-4} Pa·s at
7 353.15 K. Moreover, heat loss may also need to be considered when an adiabatic boundary
8 cannot be provided. These factors will be further considered in our following works.

9
10 In this study, relatively low v_{in} and small power input were applied to simplify the CFD
11 calculation so that the laminar model can be used for the fluid flow (just like most of the previous
12 TO studies did [20]). Some interesting efforts have been attempted in recent literature
13 regarding the TO problem treating turbulent flow (e.g., [34,47,48]). Theoretically, the GATO
14 method developed in this study can also be used to treat turbulent flow patterns under a higher
15 power input with multiple heat sources. But the CFD computation step will be more complicated
16 and time-consuming. Moreover, the current GATO method may also be extended to real 3D
17 by dividing the design domain into a 3D matrix, the channel thickness being another
18 optimization parameter. These constitute interesting directions of our future studies.

19 20 **5.4 Effectiveness vs. limitations**

21 Based on the results and discussions above, the advantages of the present GATO method
22 may be summarized as follows: (1) a clear fluid-solid boundary owing to the explicit
23 parametrization of design variables, avoiding non-physical gray scales; (2) a direct CFD
24 analysis of designs by a FVM solver without re-meshing, ensuring the
25 conservativeness/accuracy, and with excellent parallelism; and (3) robustness of GA optimizer
26 to approach global optimal solution subjected to complex heat boundaries (non-uniform
27 heating with multiple-peak heat flux).

28
29 The parameter study presented in section 4 indicates the effectiveness and robustness of the
30 proposed GATO method by proposing optimized flow path configurations with better cooling
31 performance than the RSC heat sink. Nevertheless, some limitations of the optimized designs
32 are also shown, such as the higher pressure drop, the existence of dead volumes, and the
33 existence of numerous possible optimal configurations close to the global optimum point.
34 These problems may be treated by the post-treatment (cf. section 5.1), or by revisiting the
35 objective function (e.g., multi-objective optimization [49]) and constraints (void fraction-free).
36 Further investigations in these directions are still needed.

1 Another obvious limitation of this method is the high computation cost. With the current
2 simplifications and parameter settings of the CFD model, two or three weeks are still needed
3 to obtain an optimized configuration by GATO. But this is mainly due to the sequencing &
4 queuing of the HPC as well as the cluster-local data exchange: GA algorithm written by local
5 Matlab code while CFD simulations are performed in HPC. The “effective” calculation time is
6 about 72 hours for one GATO run, which is not prohibitive at all. A significant reduction of
7 computational time is thereby feasible by executing the GA algorithm directly in the HPC, or
8 by using some local workstations instead of the HPC.

9
10 Parameters of GA play an important role on the efficiency and rapidness of this algorithm. In
11 this study, these GA parameters were selected based on some general GA guidelines [41],
12 including the crossover type, the mutation rate, the elite number, the number of individuals in
13 each generation, etc. A detailed parametric study such as done in [30] could be really useful
14 to evaluate the separate effect of each parameter on the GA diversity and the convergence
15 speed, so as to determine the appropriate parameter settings within an acceptable
16 computational cost. This could be another direction for our following work.

17 18 19 **6. Conclusion and perspectives**

20 In this paper, a GA-based topology optimization method has been developed and tested to
21 obtain the optimal global flow channel configuration of the heat sink for convective cooling of
22 a non-uniform heating surface with multiple heat sources. Minimizing the peak temperature at
23 the heating surface (T_{peak}) is defined as the optimization objective under the constraint of
24 constant void fraction for a fully-connected fluid domain. Effects of design variables, like the
25 heat flux heterogeneity, the void fraction, the inlet velocity, and the resolution of design domain
26 on the effectiveness of the GATO method have been investigated. Thermal and hydraulic
27 performances of the optimized GATO heat sink have been compared with those of reference
28 conventional straight channel (RSC) heat sink under the same conditions. The main
29 conclusions could be drawn as follows:

- 30
- 31 • The proposed GATO method could successfully determine the optimal spatial
32 distribution of the fluid/solid elements in the design domain. The resulted meshed
33 channel circuits intentionally guide the cooling fluid to the overheating positions, leading
34 to the minimized T_{peak} of the heating surface.
 - 35 • The optimized flow configurations depend strongly on the values of design and
36 operating parameters. The robustness and the reproducibility tests also imply that

1 many “close-to-the-optima” solutions can be proposed by GATO because of the
2 insensitivity of the objective function to the global optimum at the fixed stopping criterion.

- 3 • Compared with conventional RSC heat sinks, the GATO heat sinks always achieve a
4 better thermal performance, indicated by the higher Nu number, the lower R_{th} , and the
5 better temperature uniformity at the heating surface, but at the cost of the higher
6 pressure drop. The performance improvement is more significant under more
7 heterogeneous heating conditions (higher intensity difference between heat flux peaks),
8 highlighting the strong adaptability of the developed optimization method owing to the
9 more morphologic freedom offered by GA to address unspecified problems.
- 10 • A higher matrix resolution of the design area leads to lowered T_{peak} at convergence,
11 owing to the generation of finer and more complex structures at a local level.
12 Nevertheless, a larger number of GA generations is needed thus time-consuming.
13 Regarding engineering application, the appropriate design resolution (size of the
14 element to morph) should be decided by considering both the available computing
15 resources and the fabrication capacity.

16
17 This CFD-based optimization method relies on the accuracy of numerical simulation while the
18 experimental validation of the proposed method is indispensable. This involves the simulation,
19 optimization, fabrication, experimental testing, and performance comparison of different heat
20 sink prototypes, which will be presented in our later work. Meanwhile, different objective
21 functions considering both thermal and hydraulic indicators and other constraints for GATO
22 will be also investigated in our future work.

23 24 25 **Acknowledgement**

26 This work is supported by the Chinese Scholarship Council (CSC) with the scholarship for Dr.
27 Yijun LI (No. 201908070033). Authors would like to thank CCIPL (Le Centre de calcul intensif
28 des Pays de la Loire) France, for providing the computational resources.

References

- [1] G. Türkakar, T. Okutucu-Özyurt, Dimensional optimization of microchannel heat sinks with multiple heat sources, *Int. J. Therm. Sci.* 62 (2012) 85–92. <https://doi.org/10.1016/j.ijthermalsci.2011.12.015>.
- [2] Y.S. Shao, J. Clemons, R. Venkatesan, B. Zimmer, M. Fojtik, N. Jiang, B. Keller, A. Klinefelter, N. Pinckney, P. Raina, S.G. Tell, Y. Zhang, W.J. Dally, J. Emer, C.T. Gray, B. Khailany, S.W. Keckler, Simba: Scaling Deep-Learning Inference with Multi-Chip-Module-Based Architecture, in: *Proc. 52nd Annu. IEEE/ACM Int. Symp. Microarchitecture*, ACM, New York, NY, USA, 2019: pp. 14–27. <https://doi.org/10.1145/3352460.3358302>.
- [3] X. Zhang, Z. Li, L. Luo, Y. Fan, Z. Du, A review on thermal management of lithium-ion batteries for electric vehicles, *Energy*. 238 (2022) 121652. <https://doi.org/10.1016/j.energy.2021.121652>.
- [4] E.M. Abo-Zahhad, S. Ookawara, A. Radwan, A.H. El-Shazly, M.F. El-Kady, M.F.C. Esmail, Performance, limits, and thermal stress analysis of high concentrator multijunction solar cell under passive cooling conditions, *Appl. Therm. Eng.* 164 (2020) 114497. <https://doi.org/10.1016/j.applthermaleng.2019.114497>.
- [5] V.N. Ferreira, M. Andresen, B. Cardoso, M. Liserre, Pulse-Shadowing Based Thermal Balancing in Multichip Modules, *IEEE Trans. Ind. Appl.* (2020) 1–1. <https://doi.org/10.1109/TIA.2020.2993526>.
- [6] M. Wei, Y. Fan, L. Luo, G. Flamant, Fluid flow distribution optimization for minimizing the peak temperature of a tubular solar receiver, *Energy*. 91 (2015) 663–677. <https://doi.org/10.1016/j.energy.2015.08.072>.
- [7] L. Sirisha Maganti, P. Dhar, T. Sundararajan, S.K. Das, Selecting Optimal Parallel Microchannel Configuration(s) for Active Hot Spot Mitigation of Multicore Microprocessors in Real Time, *J. Heat Transfer*. 139 (2017). <https://doi.org/10.1115/1.4036643>.
- [8] Y. Hadad, B. Ramakrishnan, R. Pejman, S. Rangarajan, P.R. Chiarot, A. Pattamatta, B. Sammakia, Three-objective shape optimization and parametric study of a micro-channel heat sink with discrete non-uniform heat flux boundary conditions, *Appl. Therm. Eng.* 150 (2019) 720–737. <https://doi.org/10.1016/j.applthermaleng.2018.12.128>.
- [9] Z. Zhang, X. Wang, Y. Yan, A review of the state-of-the-art in electronic cooling, *E-Prime - Adv. Electr. Eng. Electron. Energy*. 1 (2021) 100009. <https://doi.org/10.1016/j.prime.2021.100009>.
- [10] H.E. Ahmed, B.H. Salman, A.S. Kherbeet, M.I. Ahmed, Optimization of thermal design of heat sinks: A review, *Int. J. Heat Mass Transf.* 118 (2018) 129–153. <https://doi.org/10.1016/j.ijheatmasstransfer.2017.10.099>.
- [11] N.H. Naquiddin, L.H. Saw, M.C. Yew, F. Yusof, T.C. Ng, M.K. Yew, Overview of micro-channel design for high heat flux application, *Renew. Sustain. Energy Rev.* 82 (2018) 901–914. <https://doi.org/10.1016/j.rser.2017.09.110>.
- [12] I.A. Ghani, N.A. Che Sidik, N. Kamaruzzaman, W. Jazair Yahya, O. Mahian, The effect of manifold zone parameters on hydrothermal performance of micro-channel HeatSink: A review, *Int. J. Heat Mass Transf.* 109 (2017) 1143–1161. <https://doi.org/10.1016/j.ijheatmasstransfer.2017.03.007>.
- [13] I.A. Ghani, N.A.C. Sidik, N. Kamaruzaman, Hydrothermal performance of microchannel heat sink: The effect of channel design, *Int. J. Heat Mass Transf.* 107 (2017) 21–44. <https://doi.org/10.1016/j.ijheatmasstransfer.2016.11.031>.
- [14] Y. Li, S. Roux, C. Castelain, L. Luo, Y. Fan, Tailoring the fluid flow distribution in a parallel mini-channel heat sink under multiple-peak heat flux, *Therm. Sci. Eng. Prog.* 29 (2022) 101182. <https://doi.org/10.1016/j.tsep.2021.101182>.
- [15] F. Dugast, Y. Favennec, C. Josset, Y. Fan, L. Luo, Topology optimization of thermal fluid flows with an adjoint Lattice Boltzmann Method, *J. Comput. Phys.* 365 (2018) 376–404. <https://doi.org/10.1016/j.jcp.2018.03.040>.
- [16] J. Luo, L. Chen, A. He, W. Tao, Topology optimization of convective heat transfer by the lattice Boltzmann method, *Int. J. Numer. Methods Fluids*. 95 (2023) 421–452. <https://doi.org/10.1002/flid.5153>.

- 1 [17] S. Zeng, B. Kanargi, P.S. Lee, Experimental and numerical investigation of a mini channel forced air heat
2 sink designed by topology optimization, *Int. J. Heat Mass Transf.* 121 (2018) 663–679.
3 <https://doi.org/10.1016/j.ijheatmasstransfer.2018.01.039>.
- 4 [18] T. Dbouk, A review about the engineering design of optimal heat transfer systems using topology
5 optimization, *Appl. Therm. Eng.* 112 (2017) 841–854.
6 <https://doi.org/10.1016/j.applthermaleng.2016.10.134>.
- 7 [19] J. Alexandersen, C.S. Andreasen, A Review of Topology Optimisation for Fluid-Based Problems, *Fluids*. 5
8 (2020) 29. <https://doi.org/10.3390/fluids5010029>.
- 9 [20] A. Fawaz, Y. Hua, S. Le Corre, Y. Fan, L. Luo, Topology optimization of heat exchangers: A review, *Energy*.
10 252 (2022) 124053. <https://doi.org/10.1016/j.energy.2022.124053>.
- 11 [21] J. Zhou, M. Lu, Q. Zhao, D. Hu, H. Qin, X. Chen, Thermal design of microchannel heat sinks using a contour
12 extraction based on topology optimization (CEBTO) method, *Int. J. Heat Mass Transf.* 189 (2022) 122703.
13 <https://doi.org/10.1016/j.ijheatmasstransfer.2022.122703>.
- 14 [22] O. Sigmund, J. Petersson, Numerical instabilities in topology optimization: A survey on procedures dealing
15 with checkerboards, mesh-dependencies and local minima, *Struct. Optim.* 16 (1998) 68–75.
16 <https://doi.org/10.1007/BF01214002>.
- 17 [23] Gao Wei, An improved fast-convergent genetic algorithm, in: *IEEE Int. Conf. Robot. Intell. Syst. Signal*
18 *Process.* 2003. *Proceedings.* 2003, IEEE, n.d.: pp. 1197–1202.
19 <https://doi.org/10.1109/RISSP.2003.1285761>.
- 20 [24] J.H. Holland, Genetic Algorithms, *Sci. Am.* 267 (1992) 66–72.
21 <https://doi.org/10.1038/scientificamerican0792-66>.
- 22 [25] L. Gosselin, M. Tye-Gingras, F. Mathieu-Potvin, Review of utilization of genetic algorithms in heat transfer
23 problems, *Int. J. Heat Mass Transf.* 52 (2009) 2169–2188.
24 <https://doi.org/10.1016/j.ijheatmasstransfer.2008.11.015>.
- 25 [26] J. Gao, Z. Hu, Q. Yang, X. Liang, H. Wu, Fluid flow and heat transfer in microchannel heat sinks: Modelling
26 review and recent progress, *Therm. Sci. Eng. Prog.* 29 (2022) 101203.
27 <https://doi.org/10.1016/j.tsep.2022.101203>.
- 28 [27] M. Yoshimura, K. Shimoyama, T. Misaka, S. Obayashi, Topology optimization of fluid problems using
29 genetic algorithm assisted by the Kriging model, *Int. J. Numer. Methods Eng.* 109 (2017) 514–532.
30 <https://doi.org/10.1002/nme.5295>.
- 31 [28] K. Shimoyama, A. Komiya, Multi-objective Bayesian topology optimization of a lattice-structured heat sink
32 in natural convection, *Struct. Multidiscip. Optim.* 65 (2022) 1. <https://doi.org/10.1007/s00158-021-03092-x>.
- 33 [29] B.S. Mekki, S.P. Lynch, Voxel-Based Topology Optimization of Heat Exchanger Fins, in: *AIAA SCITECH*
34 *2022 Forum, American Institute of Aeronautics and Astronautics, Reston, Virginia, 2022.*
35 <https://doi.org/10.2514/6.2022-2445>.
- 36 [30] B.S. Mekki, J. Langer, S. Lynch, Genetic algorithm based topology optimization of heat exchanger fins
37 used in aerospace applications, *Int. J. Heat Mass Transf.* 170 (2021) 121002.
38 <https://doi.org/10.1016/j.ijheatmasstransfer.2021.121002>.
- 39 [31] J. Weber, E.D. Huckaby, D. Straub, Comparison of Shape Optimization Methods for Heat Exchanger Fins
40 Using Computational Fluid Dynamics, *Int. J. Heat Mass Transf.* 207 (2023) 124003.
41 <https://doi.org/10.1016/j.ijheatmasstransfer.2023.124003>.
- 42 [32] K. Yaji, S. Yamasaki, K. Fujita, Data-driven multifidelity topology design using a deep generative model:
43 Application to forced convection heat transfer problems, *Comput. Methods Appl. Mech. Eng.* 388 (2022)
44 114284. <https://doi.org/10.1016/j.cma.2021.114284>.
- 45 [33] Y. Joo, I. Lee, S.J. Kim, Topology optimization of heat sinks in natural convection considering the effect of
46 shape-dependent heat transfer coefficient, *Int. J. Heat Mass Transf.* 109 (2017) 123–133.
47 <https://doi.org/10.1016/j.ijheatmasstransfer.2017.01.099>.

- 1 [34] S.B. Dilgen, C.B. Dilgen, D.R. Fuhrman, O. Sigmund, B.S. Lazarov, Density based topology optimization
2 of turbulent flow heat transfer systems, *Struct. Multidiscip. Optim.* 57 (2018) 1905–1918.
3 <https://doi.org/10.1007/s00158-018-1967-6>.
- 4 [35] S. Sun, P. Liebersbach, X. Qian, 3D topology optimization of heat sinks for liquid cooling, *Appl. Therm. Eng.*
5 178 (2020) 115540. <https://doi.org/10.1016/j.applthermaleng.2020.115540>.
- 6 [36] M. Yu, X. Wang, J. Gu, S. Ruan, Z. Li, S. Qian, J. Zhang, C. Shen, A synergic topology optimization
7 approach on distribution of cooling channels and diverse-intensity heat sources for liquid-cooled heat sink,
8 *Struct. Multidiscip. Optim.* 65 (2022) 48. <https://doi.org/10.1007/s00158-021-03113-9>.
- 9 [37] S. Ozguc, L. Pan, J.A. Weibel, Topological optimization of flow-shifting microchannel heat sinks, *Int. J. Heat
10 Mass Transf.* 207 (2023) 123933. <https://doi.org/10.1016/j.ijheatmasstransfer.2023.123933>.
- 11 [38] R. Boichot, Y. Fan, A genetic algorithm for topology optimization of area-to-point heat conduction problem,
12 *Int. J. Therm. Sci.* 108 (2016) 209–217. <https://doi.org/10.1016/j.ijthermalsci.2016.05.015>.
- 13 [39] R. Boichot, L. Wang, L. Luo, Y. Fan, Cellular Automaton Methods for Heat and Mass Transfer Intensification,
14 in: *Heat Mass Transf. Intensif. Shape Optim.*, Springer London, London, 2013: pp. 141–170.
15 https://doi.org/10.1007/978-1-4471-4742-8_6.
- 16 [40] D. BHANDARI, C.A. MURTHY, S.K. PAL, GENETIC ALGORITHM WITH ELITIST MODEL AND ITS
17 CONVERGENCE, *Int. J. Pattern Recognit. Artif. Intell.* 10 (1996) 731–747.
18 <https://doi.org/10.1142/S0218001496000438>.
- 19 [41] S. Mondal, A. Tsourdos, Optimal topology for consensus using genetic algorithm, *Neurocomputing.* 404
20 (2020) 41–49. <https://doi.org/10.1016/j.neucom.2020.04.107>.
- 21 [42] Chen Li, R.A. Wirtz, Development of a high performance heat Sink Based on screen-fin technology, *IEEE
22 Trans. Components Packag. Technol.* 28 (2005) 80–87. <https://doi.org/10.1109/TCAPT.2004.843171>.
- 23 [43] OpenFoam user guide, version 7, 2019, n.d.
- 24 [44] Le Centre de Calcul Intensif des Pays de la Loire (CCIPL), (n.d.). <http://wiki.ccipl.univ-nantes.fr/>.
- 25 [45] D. Tondeur, Y. Fan, L. Luo, Constructal optimization of arborescent structures with flow singularities, *Chem.
26 Eng. Sci.* 64 (2009) 3968–3982. <https://doi.org/10.1016/j.ces.2009.05.052>.
- 27 [46] G. Hetsroni, A. Mosyak, E. Pogrebnyak, L.P. Yarin, Heat transfer in micro-channels: Comparison of
28 experiments with theory and numerical results, *Int. J. Heat Mass Transf.* 48 (2005) 5580–5601.
29 <https://doi.org/10.1016/j.ijheatmasstransfer.2005.05.041>.
- 30 [47] J. Zhao, M. Zhang, Y. Zhu, R. Cheng, L. Wang, Topology optimization of turbulent forced convective heat
31 sinks using a multi-layer thermofluid model, *Struct. Multidiscip. Optim.* 64 (2021) 3835–3859.
32 <https://doi.org/10.1007/s00158-021-03064-1>.
- 33 [48] Q. Holka, E. Toubiana, J. Cortial, B. Ghannam, M. Nemer, Density-based topology optimization of a surface
34 cooler in turbulent flow using a continuous adjoint turbulence model, *Struct. Multidiscip. Optim.* 65 (2022)
35 223. <https://doi.org/10.1007/s00158-022-03311-z>.
- 36 [49] H. Li, X. Ding, F. Meng, D. Jing, M. Xiong, Optimal design and thermal modelling for liquid-cooled heat sink
37 based on multi-objective topology optimization: An experimental and numerical study, *Int. J. Heat Mass
38 Transf.* 144 (2019) 118638. <https://doi.org/10.1016/j.ijheatmasstransfer.2019.118638>.

39